SIAM J. Applied Dynamical Systems
Vol. 15, No. 1, pp. 391–439

Nonsmooth Bifurcations of Mean Field Systems of Two-Dimensional Integrate and Fire Neurons*

Wilten Nicola† and Sue Ann Campbell†

Abstract. Mean field systems have recently been derived that adequately predict the behaviors of large networks of coupled integrate-and-fire neurons [W. Nicola and S.A. Campbell, *J. Comput. Neurosci.*, 35 (2013), pp. 87–108]. The mean field system for a network of neurons with spike frequency adaptation is typically a pair of differential equations for the mean adaptation and synaptic gating variable of the network. These differential equations are nonsmooth, and, in particular, are piecewise smooth continuous (PWSC). Here, we analyze the smooth and nonsmooth bifurcation structure of these equations and show that the system is organized around a pair of co-dimension-two bifurcations that involve, respectively, the collision between a Hopf equilibrium point and a switching manifold, and a saddle-node equilibrium point and a switching manifold. These two co-dimension-two bifurcations can coalesce into a co-dimension-three nonsmooth bifurcation. As the mean field system we study is a nongeneric piecewise smooth continuous system, we discuss possible regularizations of this system and how the bifurcations which occur are related to nonsmooth bifurcations displayed by generic PWSC systems.

Key words. nonsmooth dynamical systems, bifurcation theory, computational neuroscience, mean field systems, population density methods

AMS subject classifications. 34C23, 49J52, 37C99, 37N25

DOI. 10.1137/140985846

1. Introduction.

Recently, a class of two-dimensional integrate and fire type models have been developed which can be fit to properties of real neurons. This class of models includes the Izhikevich model [19], the quartic integrate and fire model [27], and the adaptive exponential (AdEx) integrate and fire model [2, 21]. The models in this class are far simpler to fit and simulate than traditional conductance based models. Nevertheless, these models still replicate the more complex behaviors observed in real neurons [19]. These models have been fit to several different neuron types so that the behavior of large networks of these neuron models may be studied through numerical exploration of the parameter space. For example, this approach has been used to determine the role of various parameters in the generation of adaptation induced bursting in networks of hippocampal pyramidal neurons [17, 23, 16]. While the numerical simulation of integrate and fire networks is far simpler and faster than that of conductance based models, numerical exploration of the parameter space is still a time-consuming process. Furthermore, one cannot easily perform direct bifurcation analysis on large networks.

A system of mean field equations has been derived for these large networks of two-

*Received by the editors September 11, 2014; accepted for publication (in revised form) by J. Sieber August 31, 2015; published electronically February 23, 2016.
http://www.siam.org/journals/siads/15-1/98584.html
†Applied Mathematics, University of Waterloo, 200 University Avenue West, Waterloo, ON N2L 3G1, Canada (wnicola@uwaterloo.ca, sacampbell@uwaterloo.ca).

dimensional integrate and fire neurons [23]. This derivation assumes that the networks are all-to-all coupled and the neuronal parameters are homogeneous within the network. The resulting mean field system is a set of nonsmooth differential equations governing the first moments of the adaptation variable and the synaptic coupling variable. The mean field system of equations is analytically derived from the original network, without any further fitting. Thus, one can conduct bifurcation analysis (either analytically or numerically) on the mean field system with confidence that the results are representative of the behavior of the original network of model neurons.

However, analysis of the derived mean field system has an added level of difficulty as the system of equations is nonsmooth. Both classical bifurcation theory and the newer field of nonsmooth bifurcation theory must be used to adequately understand the behavior of the mean field system, and thus the full network. To further complicate the situation, the vast majority of work done in nonsmooth systems is primarily concerned with Filippov systems where the differential equations are completely discontinuous in specific subsets of the phase space [4, 12, 15, 20]. The mean field system, while nonsmooth, is still continuous across the phase space, and is thus a piecewise smooth continuous system, which is a significantly less studied class of systems [5, 13, 14].

Here we explore, both analytically and numerically, many of the nonsmooth bifurcations and phenomena that occur in the mean field system of equations from [23]. The primary mean field system we use is that of the Izhikevich model, with the neuronal models fit to hippocampal area CA3 pyramidal neuron data [7]. We modify the parameters slightly as the neuronal model used in [7] was an alteration of the default Izhikevich model to better fit the action potential half-width observed in the data. We use this model primarily for two reasons: it is the most analytically tractable and the parameters have been fit to neuronal data. However, as we will see, many of the nonsmooth bifurcations are present in the other models in the general class of two-dimensional adapting integrate and fire neurons. Whenever possible we present our results in terms of this general class.

2. The mean field system.

2.1. The full network.

We consider two-dimensional integrate and fire models of the form

$$\dot{v} = F(v) - w + I, \tag{1}$$

$$\dot{w} = a(bv - w), \tag{2}$$

where v represents the nondimensionalized membrane potential, and w serves as an adaptation variable. Time has also been nondimensionalized. The dynamical equations (1)–(2) are supplemented by the following discontinuities:

$$v(t^-_{spike}) = v_{peak} \rightarrow \begin{array}{rcl} v(t^+_{spike}) & = & v_{reset}, \\ w(t^+_{spike}) & = & w(t^-_{spike}) + \hat{w}. \end{array} \tag{3}$$

This particular notation was formally introduced in [27], along with a full bifurcation analysis of this general family of adapting integrate and fire neurons. Members of this family include the Izhikevich model, the adaptive exponential (AdEx) integrate and fire model, and the

quartic integrate and fire model [27]. The class of models is constrained to those that satisfy $F''(v) > 0$ and $\lim_{v\to-\infty} F'(v) < 0, \lim_{v\to\infty} F'(v) > 0$.

These neurons can be coupled together via a synaptic gating variable, $s(t)$. The gating variable typically takes the form

$$s_{ij}(t) = \sum_{t_{j,k}<t} E(t - t_{j,k}), \tag{4}$$

where $t_{j,k}$ is the time that the jth neuron fires its kth spike, j is the index of the presynaptic neuron, and i is the index of the postsynaptic neuron. The function $E(t)$ varies depending on which synaptic pulse function is used. For simplicity we restrict our attention to the exponential synapse; however, the analysis can be extended to the other synaptic types without much difficulty. For the exponential synapse, $E(t)$ is given by

$$E(t) = \lambda_s \exp\left(-\frac{t}{\tau_s}\right).$$

Given the form for $E(t)$, one can derive a differential equation for $s_i(t) = \sum_{j=1}^{N} s_{ij}(t)$, the total synaptic input to the ith neuron [9, 23]. For example, for the exponential synapse the differential equation for $s_i(t)$ is

$$\frac{ds_i(t)}{dt} = -\frac{s_i}{\tau_s} + \frac{\lambda_s}{\tau_s N} \sum_{j=1}^{N} \sum_{t_{j,k}<t} \delta(t - t_{j,k}). \tag{5}$$

For all-to-all coupling, the function $s_i(t)$ becomes identical for all the neurons, and can be replaced by a single variable $s(t)$, the global synaptic coupling function. In this case, the equations for the entire network are

$$\dot{v}_i = F(v_i) - w + I + gs(t)(e_r - v_i), \tag{6}$$

$$\dot{w}_i = \frac{1}{\tau_w}(bv_i - w_i), \tag{7}$$

$$\dot{s} = -\frac{s}{\tau_s} + \frac{\lambda_s}{\tau_s N} \sum_{j=1}^{N} \sum_{t_{j,k}<t} \delta(t - t_{j,k}), \tag{8}$$

$$v_i(t^-_{spike}) = v_{peak} \to \begin{array}{rcl} v_i(t^+_{spike}) & = & v_{reset}, \\ w_i(t^+_{spike}) & = & w_i(t^-_{spike}) + \hat{w}. \end{array} \tag{9}$$

The specific forms of $F(v)$ we consider are

$$F(v) = v(v - \alpha) \quad \text{(Izhikevich model)},$$
$$F(v) = e^v - v \quad \text{(AdEx model)},$$
$$F(v) = v^4 - \frac{2v}{\tau_w} \quad \text{(quartic model)}.$$

These forms can be arrived at through a suitable nondimensionalization of the original equations for these models [27]. Note that the nondimensionalization for the Izhikevich model differs from the one used by [27] and is from [23].

Table 1

Parameters for various network types and the mean field systems. Note that the parameters below are dimensionless, while in some of the cited sources they are in dimensional form only. The nondimensionalization for the AdEx and quartic neurons can be found in [27] while the nondimensionalization for the Izhikevich model can be found in [23].

Parameter	Izhikevich network (from [7])	AdEx network (from [2])	QIF network (from [27])
g	0–4	0–1000	0–40
I	0–0.4	-1–12	0–40
τ_s	2.6	2.06	2
τ_w	130	3.63	50
$\hat{s}$	0.8	0.5	1
$\hat{w}$	0.0189	21.92	0.36
e_r	1	5	2
α	0.62	N/A	N/A
v_{peak}	1.46	65	10
v_{reset}	0.15	-1.25	0

These networks often display bursting, a oscillatory behavior where the individual neurons alternate between firing and quiescence [7, 23]. The other common behavior is tonic firing, where the neurons all fire at a constant rate. The transition between these two behaviors is a bifurcation of the full network. Examples of this transition for networks of 1000 neurons with all-to-all coupling and parameters as in Table 1 are shown in Figure 1. In Figure 1(a) and 1(c) the neurons in the network fire spikes, and the mean-adaptation variable, w, and the synaptic coupling variable, s, both converge to a stable steady state. In Figure 1(b) and 1(d) the neurons fire synchronized bursts, and the pair of variables (w, s) converges to a steady state limit cycle, representing the oscillation between firing and quiescence that the individual neurons undergo. This occurs as the current I is decreased.

As seen in Figure 1, the network variables s and w can capture a great deal of information about the behavior of the entire network. Further, their steady state behavior undergoes a qualitative change as the parameter I is decreased. Thus, it would be advantageous to have a closed set of differential equations for these variables, as any qualitative change in the behavior of the full network should manifest itself as a bifurcation of the dynamical system for (s, w). In the following subsection, we present the mean field system for these networks. A detailed derivation can be found in [23].

2.2. The mean field system. To derive the mean field system one begins by defining the population density function, $\rho(v, w, t)$, which is a probability density function for the location of of the variables v, w in the phase space. That is, the probability of finding a neuron in the region Ω of phase space is given by integrating ρ over Ω. Starting from the full network model, one can derive (in the limit that $N \to \infty$) a partial differential equation that governs the evolution of the probability density function $\rho(v, w, t)$ and predicts the large network dynamics of the original model [24, 25]. This partial differential equation, called the population density equation, takes the form

$$\frac{\partial \rho(v, w, t)}{\partial t} = -\nabla \cdot \boldsymbol{J}(v, w, t),$$

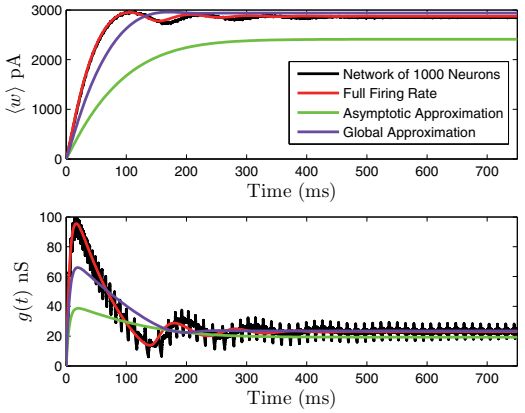

(a) Izhikevich, Tonic Firing, $I = 0.33$, $g = 0.61$ (dimensionless).

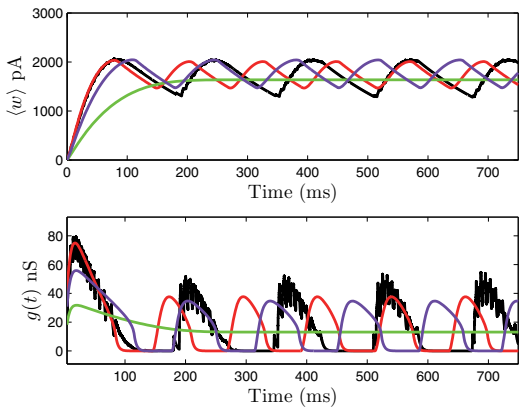

(b) Izhikevich, Bursting, $I = 0.24$, $g = 0.61$ (dimensionless).

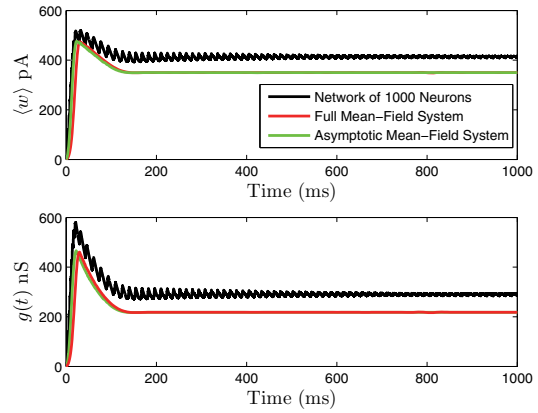

(c) AdEx, Tonic Firing, $I = 4.25$, $g = 930$ (dimensionless).

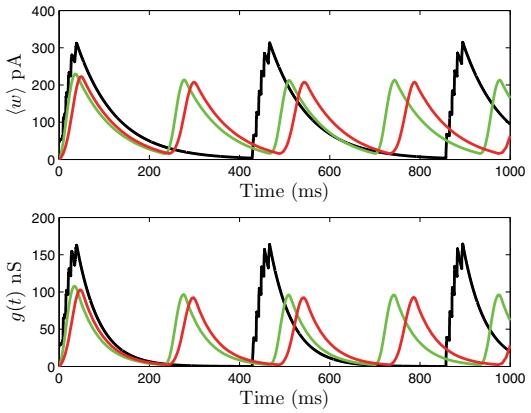

(d) AdEx, Bursting, $I = 4.25$, $g = 465$ (dimensionless).

Figure 1. *Network simulations consisting of* 1000 *neurons (black) versus the mean field system of equations* (18)–(20) *(red), the system of equations with the asymptotically simplified firing rate* (24) *(green) for a network of Izhikevich neurons* (a),(b) *and AdEx network of neurons* (c),(d). *The asymptotic firing rate,* $\langle R_i(t)\rangle \sim \sqrt{I - I^*(s,w)}\sqrt{F''(v^*(s))}$, *is a good approximation for the network of AdEx integrate and fire neuron away from the switching manifold* $I - I^*(s,w) = 0$. *This is not the case for the network of Izhikevich neuron, which is better approximated when a global approximation,* $k\sqrt{I - I^*(s,w)}\sqrt{F''(v^*(s))}$, *to the firing rate is used (green). The parameter* k *in this global approximation is fitted to approximate the full firing rate for a large set of* (s,w).

$$\boldsymbol{J}(v,w,t) = \begin{pmatrix} J_V(v,w,t) \\ J_W(v,w,t) \end{pmatrix} = \rho(v,w,t) \begin{pmatrix} F(v) - w + I + gs(e_r - v) \\ a(bv - w) \end{pmatrix},$$

where the term $\boldsymbol{J}(v,w,t)$ is referred to as the flux. The discontinuities and discrete jumps in the model neurons impose a boundary condition on the flux:

$$J_V(v_{peak}, w, t) = J_V(v_{reset}, w + \hat{w}, t).$$

This PDE is coupled to an ODE for s, given by

$$s' = -\frac{s}{\tau_s} + \frac{\lambda_s}{\tau_s}\int_W J_V(v_{peak}, w, t)\, dw. \tag{10}$$

In order to reduce this system to a small, closed set of ordinary differential equations, one has to apply a series of approximations. The derivation is somewhat lengthy; thus we refer the reader to [23] for the exact details. The primary steps are a first order moment closure assumption which yields the system

$$\frac{\partial \rho_V(v,t)}{\partial t} = -\frac{\partial}{\partial v}\left[G(v, s, \langle w\rangle)\rho_V(v,t)\right], \tag{11}$$

$$\langle w\rangle' = \frac{1}{\tau_w}(b\langle v\rangle - \langle w\rangle) + \frac{\lambda_w}{\tau_w}G(v_{peak}, s, \langle w\rangle)\rho_V(v_{peak}, t), \tag{12}$$

$$s' = -\frac{s}{\tau_s} + \frac{\lambda_s}{\tau_s}G(v_{peak}, s, \langle w\rangle)\rho_V(v_{peak}, t), \tag{13}$$

where $\lambda_w = \tau_w \hat{w}$ and

$$G(v, s, w) \overset{def}{=} F(v) - w + I + gs(e_r - v). \tag{14}$$

Defining $\epsilon = 1/\tau_w$, and $\gamma = \tau_s/\tau_w$, one can use the new time variable $\hat{t} = \epsilon t$ to derive the "slow" system

$$\epsilon\frac{\partial \rho_V(v,\hat{t})}{\partial \hat{t}} = -\frac{\partial}{\partial v}\left[G(v, s, \langle w\rangle)\rho_V(v,\hat{t})\right], \tag{15}$$

$$\frac{d\langle w\rangle}{d\hat{t}} = b\langle v\rangle - \langle w\rangle + \lambda_w G(v_{peak}, s, \langle w\rangle)\rho_V(v_{peak}, \hat{t}), \tag{16}$$

$$\frac{ds}{d\hat{t}} = \gamma^{-1}\left(-s + \lambda_s G(v_{peak}, s, \langle w\rangle)\rho_V(v_{peak}, \hat{t})\right). \tag{17}$$

Solving the $O(1)$ problem and using the fact that $\rho_V(v,t)$ is a density (and hence normalized to 1) gives the mean field equations (in the original time scale)

$$s' = -\frac{s}{\tau_s} + \frac{\lambda_s}{\tau_s}\langle R_i(t)\rangle, \tag{18}$$

$$w' = -\frac{w}{\tau_w} + \frac{\lambda_w}{\tau_w}\langle R_i(t)\rangle, \tag{19}$$

$$\langle R_i(t)\rangle = \begin{cases} \left[\int_V \frac{dv}{F(v)-w+I+gs(e_r-v)}\right]^{-1} & \text{if} \quad H(w,s) > 0, \\ 0 & \text{if} \quad H(w,s) \le 0. \end{cases} \tag{20}$$

Here s and w correspond to the mean network adaptation and global synaptic coupling variable and we have used (14). Note that we have omitted the $\langle\rangle$ brackets denoting the average value of w present in [23] for simplicity and clarity. Additionally, we have set $b = 0$ as one can show with suitable nondimensionalization that it is small [23] and has been found to be unimportant with regards to the dynamics in standard parameter regimes in [8]. The function $\langle R_i(t)\rangle$ is

the instantaneous network averaged firing rate, as a function of s and w. The function H determines when the integral in (20) is well-defined. It defines *switching manifold* of the nonsmooth system (18)–(20).

One can derive an expression for the switching manifold equation by determining when the denominator in (20) first becomes zero somewhere in the s, w phase space. Recalling (14), we must find the minimum of $G(v, s, w)$, for $v \in [v_{reset}, v_{peak}]$, regarding s and w as fixed parameters. For the general class of models studied in [27], the function $F(v)$ is assumed to be strictly convex; that is, $F''(v) > 0$. It follows that $G(v, s, w)$ is also strictly convex as a function of v, and hence its minimum on $[v_{reset}, v_{peak}]$ occurs at a critical point. The critical points (as a function of v) are given by solving

$$\begin{aligned} \frac{\partial G}{\partial v} &= F'(v) - gs = 0 \Rightarrow, \\ F'(v^*(s)) &= gs. \end{aligned} \tag{21}$$

Thus $v^*(s)$ is the value of v at which G has a minimum. It may be the case that $v^* \notin [v_{reset}, v_{peak}]$. We will primarily ignore this particular case as typical parameter values usually ensure that $v^* \in [v_{reset}, v_{peak}]$.

The minimum value defines the function H,

$$H(s, w) = G(v^*(s), s, w) = F(v^*(s)) - w + gs(e_r - v^*(s)) + I, \tag{22}$$

and the switching manifold equation

$$0 = H(s, w) = I - w + F(v^*(s)) + gs(e_r - v^*(s)) = I - I^*(s, w).$$

This latter expression is useful as we can think of I^* as an s- and w-dependent rheobase current. Anywhere in the phase space where $I - I^*(s, w) > 0$ the network is firing with mean firing rate given by

$$\langle R_i(t) \rangle = \left[\int_V \frac{dv}{F(v) - w + I + gs(e_r - v)} \right]^{-1}. \tag{23}$$

Anywhere that $I - I^*(s, w) \leq 0$ the network is quiescent and the mean firing rate is 0.

There are a couple of important facts to note before we proceed further. First of all, $I^*(0, 0) = I_{rh}$, the rheobase current for the uncoupled, nonadapting neuron, which is governed by the equation

$$\dot{v} = F(v) + I.$$

Based on the assumptions made on $F(v)$ in [27], this model neuron has a type-I firing profile. Additionally, given that $I^*(0, 0) = -F(v^*(0))$, we have the following:

$$F(v^*(0)) = -I_{rh}.$$

These two facts will prove important for our later analysis.

To conclude we display some expressions for specific models. The rheobase currents are given by

$$I^*(s,w) = w - gse_r + \frac{(\alpha+gs)^2}{4} \quad \text{(Izhikevich)},$$
$$I^*(s,w) = w - gse_r + (1+gs)(\log(1+gs)-1) \quad \text{(AdEx)},$$
$$I^*(s,w) = w - gse_r + 3\left(\frac{gs+2a}{4}\right)^{\frac{4}{3}} \quad \text{(quartic)},$$

with corresponding minimum values of G:

$$v^*(s) = \frac{\alpha+gs}{2},$$
$$v^*(s) = \log(1+gs),$$
$$v^*(s) = \left(\frac{gs+2a}{4}\right)^{1/3}.$$

For the Izhikevich model, the mean firing rate can be evaluated analytically:

$$\langle R_i(t)\rangle = \frac{\sqrt{I-I^*(s,w)}}{\arctan\left(\frac{v_{peak}-\frac{1}{2}(\alpha+gs)}{\sqrt{I-I^*(s,w)}}\right) - \arctan\left(\frac{v_{reset}-\frac{1}{2}(\alpha+gs)}{\sqrt{I-I^*(s,w)}}\right)} \quad \text{(Izhikevich mean firing rate)}.$$

For the other models, the firing rate must be evaluated numerically. This can be done by integrating (23) over $[v_{reset}, v_{peak}]$ treating w, and s as fixed parameters at each time step. This approach can be used to numerically analyze the bifurcation types of these equations using numerical bifurcation software, such as MATCONT [6]. However, the numerical integration method should be of high enough order accuracy for the numerical continuation results to be trusted.

Given the mean field system described above, one should consider whether numerical bifurcation or analytical approaches should be taken. Numerical bifurcation analysis can yield results which are accurate throughout the phase space, but require choosing a particular model and determining which parameters to fix and which to vary. Analytical methods can yield model independent results and give insight into the role of various parameters in system behavior; however, they are often restricted to particular regions of the parameter space and/or phase space, as we shall see.

3. Analytical results.

In order to proceed analytically, we need to sacrifice some of the complexity of the original mean field system. In particular, as the usual formulas of $\langle R_i(t)\rangle$ are difficult to deal with analytically, we need to approximate the firing rate with a simpler alternative. The approximation will be provided by the following theorem.

Theorem 1. *Suppose that $F''(v) > 0$ and $F(v)$ has a unique minimum, v^*. If $v^* \in [v_{reset}, v_{peak}]$, and $M = \max\{|v_{peak}-v^*|, |v_{reset}-v^*|\}$ is sufficiently small, then $\langle R_i(t)\rangle$ has the leading order behavior*

$$\langle R_i(t)\rangle \sim \frac{1}{\sqrt{2}\pi}\sqrt{F''(v^*(s))}\sqrt{I-I^*(s,w)}, \quad I-I^*(s,w)\to 0. \tag{24}$$

This basic result follows from what is effectively Laplace's method for integrals. The proof can be found in Appendix A. This reduction is valid when $I - I^*(s,w)$ is small, that is, when the dynamics are near the region in the (s,w) plane where they become nonsmooth. We note that a similar approximation appears in [9, 10]. However, to the best of our knowledge the nonsmooth nature of those equations has not been explored. For example, (3.6)–(3.7) in [10] are similar to ours; however, the interpretation for those particular equations was for the firing rate of an E/I coupled pair of neurons.

For example, for the Izhikevich neuron, we have the following:

$$\langle R_i(t)\rangle \sim \frac{1}{\pi}\sqrt{I - I^*(s,w)} \quad \text{as} \quad I - I^*(s,w) \to 0 \tag{25}$$

while for the AdEx, we have

$$\langle R_i(t)\rangle \sim \frac{1}{\pi}\sqrt{\frac{1+gs}{2}}\sqrt{I - I^*(s,w)} \quad \text{as} \quad I - I^*(s,w) \to 0, \tag{26}$$

where the switching manifolds differ from neuron to neuron. One can see the validity of the approximations in Figure 1 which compares the behavior of full network simulations with that of the mean field model using the true firing rate and asymptotic approximation. The validity is further studied in Figure 2 which demonstrates that the difference between (23) and (24) is $o(\sqrt{I - I^*(s,w)})$ pointwise in (s,w) for the AdEX and Izhikevich systems.

The approximation (24) turns out to yield a system that is tractable to analysis of both the smooth and nonsmooth bifurcations, and shows considerable accuracy when compared with both the actual network and the original mean field system in the vicinity of the switching manifold (see Figure 1). Additionally, when the system is not near the switching manifold, one can use an ad-hoc global approximation that still preserves the bifurcation structure near the switching manifold. For example, one can use

$$\langle R_i(t)\rangle = k\sqrt{F''(v^*(s))}\sqrt{I - I^*(s,w)}, \tag{27}$$

where k is fit to globally approximate the original firing rate. This can be done, for example, by plotting $\langle R_i(t)\rangle$ versus $\sqrt{I - I^*(s(t),w(t))}$ for a small number of trajectories in the parameter plane and performing a linear fit. This is done for the Izhikevich network in Figure 1 with $k = 1/2$. One could use this approximation, for example, to conduct a rapid parameter search that is more global than the local analysis we present below. Alternative approaches for a global fit are also possible. The advantage of the approximation (27) is that it preserves the location of the co-dimension-two nonsmooth bifurcation points we describe in section 4.

With the simplification (24), the approximate mean field system that we analyze is given by

$$\dot{s} = f(s,w) = -\frac{s}{\tau_s} + \frac{\lambda_s}{\tau_s}\langle R_i(t)\rangle, \tag{28}$$

$$\dot{w} = g(s,w) = -\frac{w}{\tau_w} + \frac{\lambda_w}{\tau_w}\langle R_i(t)\rangle, \tag{29}$$

$$\langle R_i(t)\rangle = \begin{cases} \sqrt{F''(v^*(s))}\sqrt{I - I^*(s,w)}, & I - I^*(s,w) > 0, \\ 0, & I - I^*(s,w) \le 0, \end{cases} \tag{30}$$

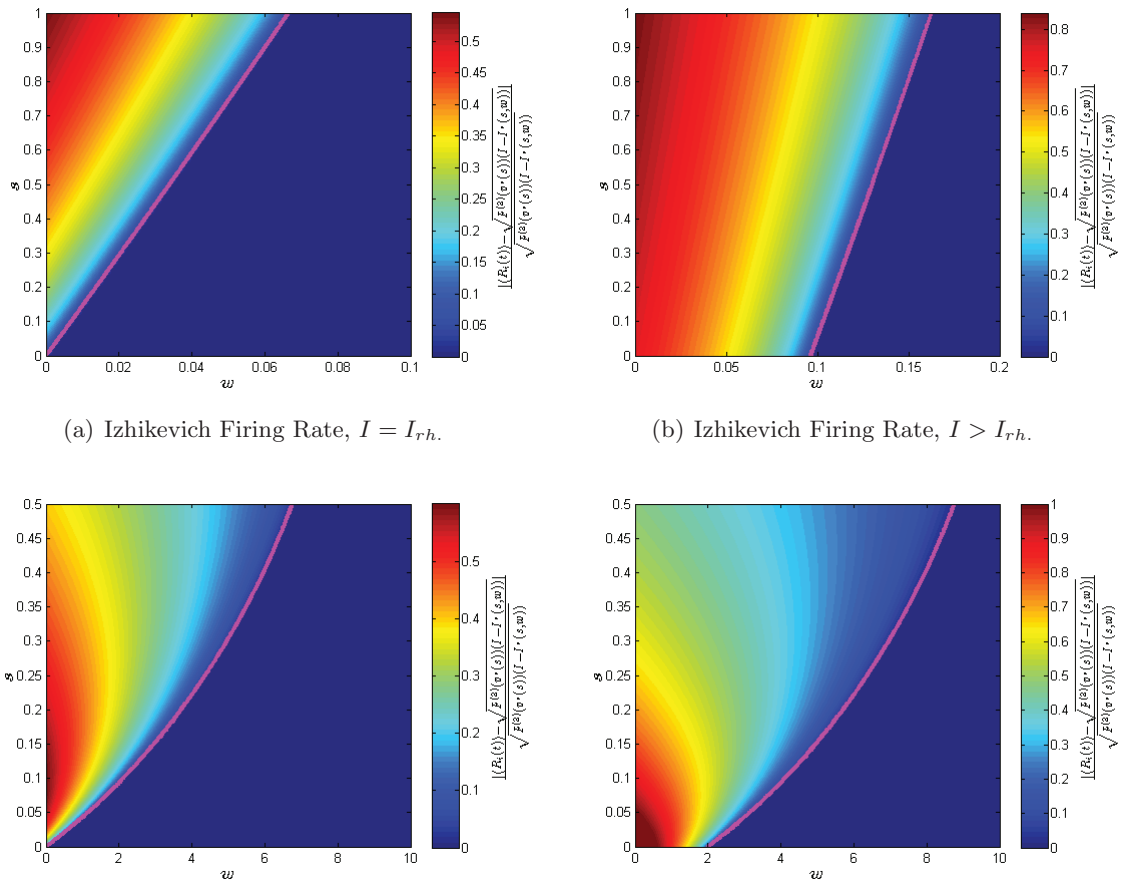

(a) Izhikevich Firing Rate, $I = I_{rh.}$

(b) Izhikevich Firing Rate, $I > I_{rh.}$

(c) AdEx Firing Rate, $I = I_{rh.}$

(d) AdEx Firing Rate, $I > I_{rh.}$

Figure 2. *Variation with (s, w) of the relative error in using the leading order asymptotic expansion, $\langle R_i(t) \rangle \sim \sqrt{F''(v^*(s))}\sqrt{I - I^*(s,w)}$, for the firing rate. There is always a neighborhood in the vicinity of the switching manifold, $I - I^*(s,w) = 0$ (magenta curve), where the firing rate is well approximated by the asymptotic expansion. This is the neighborhood where the nonsmooth bifurcations occur and to which we restrict our analysis.*

where the switching manifold varies depending on which neuron model is used and we have absorbed any constant terms into λ_s and λ_w. In the following, we will refer to (28)–(30) as the reduced mean field system. The system is smooth and has derivatives of all orders everywhere except on the switching manifold, i.e., when $I - I^*(s,w) = 0$. On the switching manifold, the system is continuous but not differentiable. Thus, this is a piecewise-smooth continuous (PWSC) system. Equivalently, it has a uniform order of discontinuity of 1 [5]. Note that the derivatives of the vector field diverge at the switching manifold. Thus one cannot simply unfold the system around a boundary equilibrium bifurcation points as is often done in the literature [13], at least not without including the relevant square-root terms.

In the following sections we will carry out a detailed bifurcation study of the mean field system (28)–(29). Before proceeding we consider when our results will give information about

the coupled PDE-ODE system (11)–(13) and hence about the original large network model. It is straightforward to see that an equilibrium point of the mean field system is a leading order approximation (as $I - I^*(s,w) \to 0$) of an equilibrium point of the full mean field system (18)–(20). Further, any equilibrium point of the full mean field system corresponds to an $O(1)$ (w.r.t. ϵ) approximation of a steady state solution of the PDE-ODE system.

To study how the stability of the steady states of the two systems corresponds we apply a procedure originally developed in [1]. We linearize the coupled PDE-ODE system around the asynchronous steady state with steady state firing rate $\langle R \rangle$ and determine the spectral equation for the linear operator of the linearized system. Analysis of this spectral equation leads to the following theorem.

Theorem 2. *Consider the coupled PDE-ODE system given by (11)–(13). The spectral equation of the linearization of this system about the asynchronous steady state is given by*

(31)
$$\left(e^{\mu/\overline{\langle R\rangle}} - 1\right)\left(\mu + \frac{1}{\tau_s}\right)\left(\mu + \frac{1}{\tau_w}\right) - \left(\mu + \frac{1}{\tau_s}\right)\left(\frac{\lambda_w}{\tau_w}\mu\hat{B}(\mu)\right) - \left(\mu + \frac{1}{\tau_w}\right)\left(\frac{\lambda_s}{\tau_s}\mu\hat{A}(\mu)\right) = 0,$$

where

$$\hat{A}(\mu) = \int_0^1 e^{\mu y/\overline{\langle R\rangle}} \frac{g(e_r - \eta^{-1}(y))}{G(\eta^{-1}(y), \lambda_s\overline{\langle R\rangle}, \lambda_w\overline{\langle R\rangle})}\, dy, \tag{32}$$

$$\hat{B}(\mu) = \int_0^1 e^{\mu y/\overline{\langle R\rangle}} \frac{-1}{G(\eta^{-1}(y), \lambda_s\overline{\langle R\rangle}, \lambda_w\overline{\langle R\rangle})}\, dy, \tag{33}$$

$$y = \eta(v) = \int_{v_{reset}}^{v} \frac{\overline{\langle R\rangle}\, dv'}{G(v', \lambda_s\overline{\langle R\rangle}, \lambda_w\overline{\langle R\rangle})}. \tag{34}$$

Equation (31) has a countable set of solutions, μ_n. Furthermore, $\Re(\mu_n) < 0$ for ϵ and $I - I^*(\lambda_s\langle R\rangle, \lambda_w\langle R\rangle)$ sufficiently small with $g\lambda_s(e_r - v^*(0)) - \lambda_w\gamma > 0$. There is also another pair of solutions which are given to leading order in ϵ by the solution to

(35)
$$0 = (\mu_1+\gamma^{-1})(\mu_1+1) - \lambda_w(\mu_1+\gamma^{-1})\frac{\partial\langle R_i(t)\rangle}{\partial w}\bigg|_{(\lambda_s\overline{\langle R\rangle}, \lambda_w\overline{\langle R\rangle})} - \gamma^{-1}\lambda_s(\mu_1+1)\frac{\partial\langle R_i(t)\rangle}{\partial s}\bigg|_{(\lambda_s\overline{\langle R\rangle}, \lambda_w\overline{\langle R\rangle})},$$

which is the eigenvalue equation for the mean field system when one back substitutes for $\mu_1 = \mu/\epsilon + O(\epsilon)$ to leading order (28)–(29) when $I - I^*(s,w) > 0$.

The proof of Theorem 2, while lengthy, is fairly standard and is contained in Appendix B. Plainly speaking, if $\tau_s = \gamma\tau_w$, and $\epsilon = 1/\tau_w$ and $I - I^*(\lambda_s\langle R\rangle, \lambda_w\langle R\rangle)$ are sufficiently small, then the stability properties of the asynchronous steady state(s) of (11)–(13) are identical to the stability properties of the corresponding equilibrium point(s) of (28)–(30). Thus, a bifurcation analysis of (28)–(30) determines the bifurcations of the steady states of (11)–(13) provided that the requirements of Theorems 1 and 2 hold. Of course, a full bifurcation analysis of (11)–(13) would require the infinite-dimensional center manifold theorem. In this paper we only concern ourselves with the mean field system (28)–(30).

3.1. Existence and linear stability of equilibria.

The equilibria of the mean field equations (28)–(29) depend on the sign of $I - I^*(s,w)$.

If $I - I^*(s,w) \leq 0$, then the only equilibrium point is the trivial solution, $e_0 = (0,0)$, which is a stable node. This equilibrium corresponds to all the neurons being quiescent, $\langle R_i(t) \rangle = 0$, and thus we will refer to it as the nonfiring solution. It will only exist when the origin of the phase space lies in the region where $I - I^*(0,0) \leq 0$, which corresponds to $I \leq I_{rh}$. Alternatively, in the language of nonsmooth dynamical systems theory, e_0 is virtual if $I > I_{rh}$ and real if $I \leq I_{rh}$ [5].

If $I - I^*(s,w) > 0$, nontrivial equilibria (s,w) may exist. If they do, then s, w must satisfy

$$s = \lambda_s \sqrt{F''(v^*(s))} \sqrt{I - I^*(s,w)}, \tag{36}$$

$$w = \lambda_w \sqrt{F''(v^*(s))} \sqrt{I - I^*(s,w)}. \tag{37}$$

Equations (36) and (37) yield the following relationship:

$$w = \frac{\lambda_w}{\lambda_s} s = \eta s. \tag{38}$$

Thus the equilibria are given by $(s, \eta s)$ where s satisfies the nonlinear equation

$$\frac{s}{\sqrt{F''(v^*(s))}} = \lambda_s \sqrt{I - I^*(s, \eta s)}. \tag{39}$$

We will label solutions to (39) as $\bar{s}$, and the full steady states as $e = (\bar{s}(g,I), \eta \bar{s}(g,I))$. Note that (36) implies that $\bar{s} = \lambda_s \sqrt{I - I^*(\bar{s}, \eta \bar{s})} \sqrt{F''(v^*(\bar{s}))} \geq 0$. Thus for an equilibrium to be a valid, it must satisfy $s \geq 0$ (which implies $w \geq 0$).

The equilibrium condition (39) for the quartic and AdEx models yields nonlinear equations without analytic closed form solutions. However, one can apply a power series (assuming that $\bar{s}$ is small) to come up with an approximation to the steady solutions. This series is justified by the fact that when one considers the steady state conditions on $\bar{s}$ and $\bar{w}$, $\bar{s}$ being small is equivalent to the equilibrium point being in the vicinity of the switching manifold. Note that v^* is actually a function of gs, as opposed to just s, as it is given by solving the algebraic equation (21). Thus, we can write down the following expansions for $v^*(s)$ and $F(v^*(s))$:

$$v^*(s) = v^*(0) + v^{*\prime}(0) gs + O((gs)^2), \tag{40}$$

$$\begin{aligned} F(v^*(s)) &= F(v^*(0)) + v^{*\prime}(0) \frac{(gs)^2}{2} + O((gs)^3) \\ &= -I_{rh} + v^{*\prime}(0) \frac{(gs)^2}{2} + O((gs)^3), \end{aligned} \tag{41}$$

where (41) can be derived using the relationship (21). Using these expansions in (39), we arrive at the following equation for the equilibria:

$$\begin{aligned} \frac{s^2}{\lambda_s^2 F''(v^*(0))} &= I - I_{rh} - v^{*\prime}(0) \frac{(gs)^2}{2} + gs(e_r - v^*(0)) - \eta s, \\ 0 &= s^2 \left(\frac{1}{F''(v^*(0)) \lambda_s^2} + \frac{g^2}{2F''(v^*(0))} \right) + s\left(\eta - g(e_r - v^*(0))\right) + I_{rh} - I + O(s^3), \\ 0 &= A_2(g) s^2 + A_1(g) s + A_0 + O(s^3). \end{aligned}$$

Neglecting the higher order terms, this equation yields two solution branches:

$$\bar{s}_\pm = -\frac{A_1(g)}{2A_2(g)} \pm \sqrt{\frac{A_1(g)^2}{4A_2(g)^2} - \frac{A_0}{A_2(g)}}.$$

We will denote the corresponding equilibria as $\bar{e}_\pm = (\bar{s}_\pm, \bar{w}_\pm) = (\bar{s}_\pm, \eta\bar{s}_\pm)$. Defining the new parameters

$$\tilde{I} = -\frac{A_0}{A_2(g)} = \frac{I - I_{rh}}{A_2(g)}, \tag{42}$$

$$\beta = -\frac{A_1(g)}{2A_2(g)} = \frac{g(e_r - v^*(0)) - \eta}{2A_2(g)}, \tag{43}$$

$$= \frac{(e_r - v^*(0))}{2A_2(g)}\left(g - \frac{\eta}{e_r - v^*(0)}\right) = M(g)(g - g^*), \tag{44}$$

the s variable of the solution branches may be written as

$$\bar{s}_\pm(\beta, \tilde{I}) = \beta \pm \sqrt{\beta^2 + \tilde{I}}. \tag{45}$$

Note that $A_2(g) > 0$. Further, since $v^*(0)$ is the minimum of $F(v)$ and the reversal potential for an excitatory synapse is above the resting membrane potential, v_r, we have $e_r > v_r > v^*(0)$. It follows that $M(g)$ is a strictly positive function.

The expressions above give the simplest approximation for the nontrivial equilibria of the two dimensional integrate and fire models. In fact, the approximation is exact in the case of the Izhikevich model as all higher order terms in the expansions (40)–(41) vanish. The exact expressions for the Izhikevich model are given by

$$\bar{s}_\pm(g, I) = \frac{-(\eta - g(e_r - \frac{\alpha}{2})) \pm \sqrt{(\eta - g(e_r - \frac{\alpha}{2}))^2 + 4(I - \frac{\alpha^2}{4})(\frac{1}{\lambda_s^2} + \frac{g^2}{4})}}{\frac{1}{\lambda_s^2} + \frac{g^2}{4}}.$$

Introducing the parameters

$$\tilde{I} = \frac{(I - \frac{\alpha^2}{4})}{\frac{1}{\lambda_s^2} + \frac{g^2}{4}}, \tag{46}$$

$$\beta = -\frac{(\eta - g(e_r - \frac{\alpha}{2}))}{2(\frac{1}{\lambda_s^2} + \frac{g^2}{4})}, \tag{47}$$

the steady states can again be written in the form (45). Note, as a check of consistency, that $I_{rh} = \frac{\alpha^2}{4}$, and $v^*(0) = \frac{\alpha}{2}$ for the Izhikevich model.

Based on the form (45) and the fact that $A_2(g) > 0$, it is straightforward to show the signs of $s_\pm$ are as shown in Figure 3(a). Since we require the equilibrium solutions to be positive, $e_\pm$ will have different regions of existence depending on the values of β and $\tilde{I}$. In particular, both equilibrium points exist when $I < I_{rh}$ and $g > \frac{\eta}{e_r - v^*(0)}$ in a wedge-shaped region given

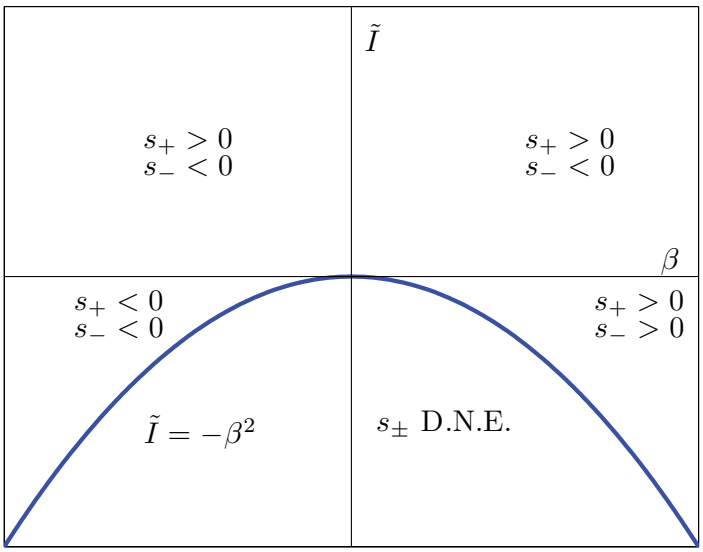

(a) $(\beta, \tilde{I})$ plane.

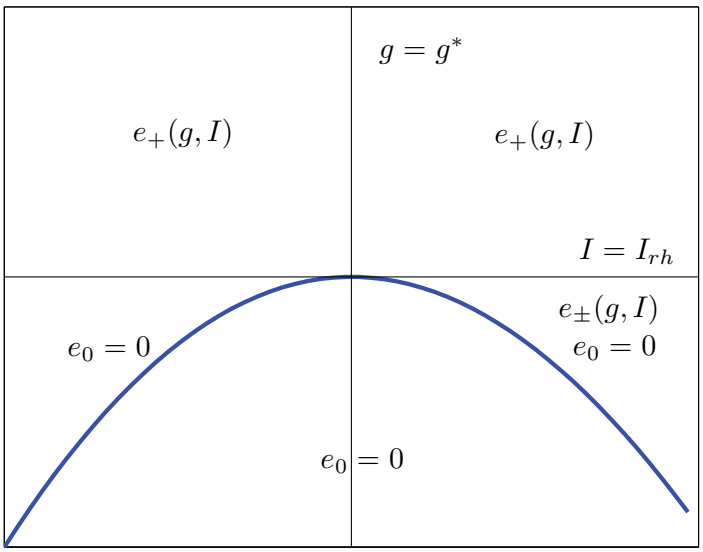

(b) (g, I) plane.

Figure 3. *The existence of equilibria for the mean field system.* (a) *The sign of the s component of the nontrivial equilibria, in the $(\beta, \tilde{I})$ parameter plane. s_+ is positive in the first two quadrants and in a narrow wedge-shaped region in the fourth quadrant. s_- is also positive in this wedge-shaped region.* (b) *The existence of the trivial and nontrivial equilibria for the Izhikevich model in the g, I parameter space. The nontrivial equilibrium $e_+(g, I)$ only exists in the region $I > \alpha^2/4$, and for $I < \alpha^2/4$ in the wedge-shaped region of the fourth quadrant indicated. The nontrivial equilibrium $e_-(g, I)$ only exists in this wedge-shaped region. The trivial (nonfiring) equilibrium e_0 only exists for $I \leq \alpha^2/4$.*

by $\beta^2 + \tilde{I} > 0$. Only e_+ exists when $I > I_{rh}$. Neither solution exists in other parts of the parameter space. The regions of existence of $e_\pm$ and the nonfiring solution are shown for the Izhikevich model in Figure 3(b).

Away from the switching manifold, we can analyze the smooth bifurcations of the equilibria via linearization. The nonfiring solution does not undergo any smooth bifurcations, as when it exists it lies in the region of phase space governed by the equations

$$s' = -\frac{s}{\tau_s},$$
$$w' = -\frac{w}{\tau_w}.$$

Thus the nonfiring solution is asymptotically stable when it exists and does not lie on the switching manifold, i.e., for $I < I_{rh}$. The nontrivial equilibria $e_\pm$ exist in the region of the phase space corresponding to $I - I^*(s,w) > 0$. In this case the Jacobian of the reduced mean field system becomes

$$J(s) = \begin{pmatrix} -\frac{1}{\tau_s} + \frac{\lambda_s}{\tau_s}\left(\frac{g\lambda_s(e_r - v^*(s))F''(v^*(s))}{2s} + \frac{s}{2F''(v^*(s))\lambda_s}F'''(v^*(s))v^{*\prime}(s)\right) & -\frac{\lambda_s^2 F''(v^*(s))}{2s\tau_s} \\ \frac{\lambda_w}{\tau_w}\left(\frac{g\lambda_s(e_r - v^*(s))F''(v^*(s))}{2s} + \frac{s}{2F''(v^*(s))\lambda_s}F'''(v^*(s))v^{*\prime}(s)\right) & -\frac{1}{\tau_w} - \frac{\lambda_w\lambda_s F''(v^*(s))}{2s\tau_w} \end{pmatrix}$$

after one takes into account the steady state condition $sF''(v^*(s))/\lambda_s = \sqrt{I - I^*(s,\eta s)}$. The trace and determinant are given by the following:

$$\begin{aligned} \mathrm{Tr}(J) &= -\frac{F''(v^*(s))}{s}\left[\left(\frac{1}{\tau_s} + \frac{1}{\tau_w}\right)\frac{s}{F''(v^*(s))}\right. \\ &\quad \left. - \frac{\lambda_s^2}{2\tau_s}\left(g(e_r - v^*(s)) + \frac{s^2 v^{*\prime}(s)F'''(v^*(s)))}{\lambda_s^2 F''(v^*(s))^2} - \eta\frac{\tau_s}{\tau_w}\right)\right], \\ \mathrm{Det}(J) &= \frac{F''(v^*(s))}{s\tau_s\tau_w}\left[\frac{s}{F'''(v^*(s))} + \frac{\lambda_w\lambda_s}{2} - \frac{\lambda_s^2}{2}(g(e_r - v^*(s)) - \frac{s^2 v^{*\prime}(s)F'''(v^*(s)))}{2F''(v^*(s))^2}\right]. \end{aligned}$$

We can now discuss the stability of each equilibrium in its region of existence. To begin we use the expansions (40)–(41) in the determinant:

$$\begin{aligned} \mathrm{Det}(J) &= \frac{F''(v^*(s))}{s\tau_s\tau_w}\left[\frac{s}{F''(v^*(s))} + \frac{\lambda_w\lambda_s}{2} - \frac{\lambda_s^2}{2}(g(e_r - v^*(s)) - \frac{s^2 v^{*\prime}(s)F'''(v^*(s)))}{\lambda_s^2 F''(v^*(s))^2}\right] \\ &= \frac{F''(v^*(s))}{s\tau_s\tau_w}\left(\frac{1}{F''(v^*(0))} + \frac{g^2\lambda_s^2}{2F''(v^*(0))}\right)\left(s - M(g)(g - g^*) + O(s^2)\right), \\ M(g) &= \frac{e_r - v^*(0)}{2A_2(g)}, \\ g^* &= \frac{\eta}{e_r - v^*(0)}. \end{aligned}$$

Substituting the equilibrium values of s and using the definition (43) of β, we obtain

$$\det(J)|_{\bar{s}_\pm} = \frac{F''(v^*(\bar{s}))A_2(g)\lambda_s^2}{\bar{s}\tau_s\tau_w}\left(\pm\sqrt{\beta^2 + \tilde{I}} + O(\bar{s}^2)\right). \tag{48}$$

Since the sign of $\frac{A_2(g)\lambda_s^2 F''(v^*(s))}{\tau_s \tau_w}$ is strictly positive, and the equilibria are only defined when $\bar{s} = \beta \pm \sqrt{\beta^2 + \tilde{I}} \geq 0$, we can immediately conclude that

$$\det(J)|_{s_+} \geq 0,$$
$$\det(J)|_{s_-} \leq 0$$

for small $s_\pm$. This implies that the equilibrium $\bar{e}_-$ is always an unstable saddle. The equilibrium $\bar{e}_+$, however, can be a node or a focus and its stability is determined by the trace. We will discuss this further in section 3.3. Note that these results are only valid when $\bar{s}_\pm$ is small for the QIF and AdEx models, but are globally valid for the Izhikevich model.

We can use the equations for the trace and determinant to formulate necessary conditions for the equilibria to display certain smooth bifurcations. In particular, $\det(J) = 0$ and $\mathrm{tr}(J) \neq 0$ are necessary conditions for an equilibrium to undergo a saddle-node bifurcation, while $\det(J) > 0$ and $\mathrm{tr}(J) = 0$ are necessary conditions for a Hopf bifurcation. Having both $\det(J) = 0$ and $\mathrm{tr}(J) = 0$ is a necessary condition for a Bogdanov–Takens bifurcation. Of course, to determine whether these bifurcations actually occur requires checking additional genericity conditions. In the following section, we check these conditions where possible.

3.2. The saddle-node bifurcation condition. As described above, necessary conditions for a saddle-node bifurcation are $\det(J) = 0$ and $\mathrm{tr}(J) \neq 0$. It is easy to see from (48) that the first condition is satisfied for both $e_\pm$ when $\beta^2 + \tilde{I} = 0$. It can be shown that the second condition is satisfied except at isolated points in the (g, I) parameter space as determined in section 3.3. In the following we will assume that we exclude these points.

To pursue this further, we study the existence of the equilibria. From the previous subsection, we know that $e_\pm$ both exist if $\beta^2 + \tilde{I} > 0$ and neither exists if $\beta^2 + \tilde{I} < 0$. When $\beta^2 + \tilde{I} = 0$, the two equilibria collapse into a single equilibrium, with $s = \beta$. We thus conclude that $\tilde{I} = -\beta^2$ corresponds to a two-parameter curve of saddle-node bifurcation. Rewriting this in terms of the original parameters yields the two-parameter bifurcation curve in terms of (g, I):

$$I = I_{rh} - A_2(g)M(g)^2(g - g^*)^2 + O((g - g^*)^2) \stackrel{def}{=} I_{SN}(g). \tag{49}$$

Thus, for fixed g, $I_{SN}(g)$ is the value of the current that corresponds to a saddle-node bifurcation point.

There are a few things to note about I_{SN}. First, since $A_2(g)$ is a strictly positive function, $I_{SN}(g) \leq I_{rh}$ with $I_{SN}(g) = I_{rh}$ only if $g = g^*$. Also, this curve is only defined for $g \geq g^*$ for $g - g^*$ not too large. To see this, note that the saddle-node equilibrium, given by $s_{SN} = \beta = M(g)(g - g^*)$, only exists if $\beta > 0$. Since $M(g) > 0$, s_{SN} only exists if $g \geq g^*$. We shall see later that $g = g^*$ actually corresponds to a nonsmooth co-dimension-two bifurcation point. Finally, as $A_2(g)$ is a strictly positive function, one can show by using Sotomayor's theorem [26] that the saddle-node bifurcation is generic provided that $g > g^*$. This is shown in the supplementary material (98584_01.pdf [local/web 152KB]). This immediately implies the following theorem.

Theorem 3. *The system of equations* (28)–(30) *undergoes a saddle-node bifurcation when*

$$I = I_{rh} - A_2(g)M(g)^2(g - g^*), \quad g > g^*,$$

which is exact and generic for the Izhikevich model and approximate to $O((g-g^*))^2$ *for all other models. Provided that the conditions of Theorems 1 and 2 are met, this corresponds to the asynchronous steady state of the population density system (11)–(13) having a zero eigenvalue.*

3.3. The Andronov–Hopf bifurcation condition. From the analysis of subsection 3.1, we know that only e_+ may undergo a Hopf bifurcation and that $\det(J)|_{s_+} > 0$ if $\beta^2 + \tilde{I} \neq 0$. We thus conclude that the determinant condition for the Hopf bifurcation is given by $I \neq I_{SN}(g)$. To determine a necessary condition for the Hopf bifurcation, we begin by using the expansions (40)–(41),

$$\mathrm{Tr}(J)$$

$$= -\left(\frac{1}{\tau_s}+\frac{1}{\tau_w}\right) + \frac{\lambda_s^2 F''(v^*(s))}{2s\tau_s}\left(g(e_r - v^*(s)) + \frac{s^2 v^{*\prime}(s) F'''(v^*(s)))}{\lambda_s^2 F''(v^*(s))^2} - \eta\frac{\tau_s}{\tau_w}\right) \tag{50}$$

$$= -\frac{F''(v^*(s))}{\tau_s s}\left(\frac{1}{F''(v^*(0))} + \frac{\gamma}{F''(v^*(0))} + \frac{g^2\lambda_s^2}{2F''(v^*(0))}\right)\left[s - N(g)(g-\bar{g}) + O(s^2)\right], \tag{51}$$

$$N(g)$$

$$= \frac{\lambda_s^2(e_r - v^*(0))}{2}\left(\frac{1}{F''(v^*(0))} + \frac{\gamma}{F''(v^*(0))} + \frac{g^2\lambda_s^2}{2F''(v^*(0))}\right)^{-1}, \tag{52}$$

$$\bar{g} = \frac{\eta}{e_r - v^*(0)}\frac{\tau_s}{\tau_w}. \tag{53}$$

Note that the first term is strictly negative and $N(g)$ is a strictly positive function. Setting the trace to zero and using (42)–(45), which define $\tilde{I}, \beta$, and $\bar{s}_+$, yields

$$\begin{aligned} \bar{s}_+ &= N(g)(g-\bar{g}) + O((g-\bar{g})^2) \\ &\Rightarrow M(g)^2(g-g^*)^2 + \frac{I - I_{rh}}{A_2(g)} = (N(g)(g-\bar{g}) - M(g)(g-g^*))^2 \end{aligned}$$

to lowest order in $\bar{s}$. Solving for I gives

$$I = I_{rh} + A_2(g)\left[N(g)^2(g-\bar{g})^2 - 2M(g)N(g)(g-\bar{g})(g-g^*)\right] + O((g-\bar{g})^2) \stackrel{def}{=} I_{AH}(g). \tag{54}$$

We thus conclude that if $I = I_{AH}(g)$ and $I \neq I_{SN}(g)$, then the equilibrium $\bar{s}_+$ has a pair of pure imaginary eigenvalues.

Recall that $N(g)$, $M(g)$, and $A_2(g)$ are positive functions. Further, it is easy to check that $N(g) < M(g)$. This leads to several observations. First, since the third equation in the sequence above can only be satisfied if $N(g)(g-\bar{g}) > M(g)(g-g^*)$, it follows that if $g^* \leq \bar{g}$, then no Hopf bifurcation occurs. Second, from the first equation in the sequence above we must have $g \geq \bar{g}$ in order for the equilibrium s_+ to exist at the Hopf bifurcation. When $g = \bar{g}$, $s_+ = 0$ and $I_{AH} = I_{rh}$. We shall see later that the point $I = I_{rh}$, $g = \bar{g}$ is a co-dimension-two nonsmooth bifurcation point. Finally, if $\bar{g} \leq g \leq g^*$, then $I_{AH} \geq I_{rh}$ with $I_{AH} = I_{rh}$ only if $g = \bar{g}$. If $g > g^*$, then it is possible for $I = I_{AH}(g)$ to intersect $I = I_{rh}$. We denote by $\hat{g}$ the value of g at the intersection point, if it exists.

We can now determine the stability of the equilibrium e_+ by studying the trace equation (51). Since the first term in this equation is strictly negative wherever it is defined (when

$\bar{e}_+$ exists), the sign of the trace is determined by $\bar{s}_+ - N(g)(g-\bar{g})$. Since $\bar{s}_+$ and $N(g)$ are positive, it follows from the discussion above that when $g^* \leq \bar{g}$ the trace is negative, and hence $\bar{e}_+$ is asymptotically stable, wherever it exists. If $\bar{g} \leq g^*$, then the trace is negative (and $\bar{e}_+$ is asymptotically stable) if $g < \bar{g}$ or $g > \bar{g}$ and $I > I_{AH}(g)$. The trace is positive (and $\bar{e}_+$ is unstable) if $g > \bar{g}$ and $I < I_{AH}$. Note that if I is sufficiently close to I_{AH}, then $\bar{e}_+$ will have a pair of complex conjugate eigenvalues.

In summary, for fixed g with $g > \bar{g}$ and $\bar{g} < g^*$, the equilibrium e_+ undergoes a Hopf bifurcation at $I = I_{AH}(g)$ if $I \neq I_{SN}(g)$. Further, we can now state completely the conditions for the saddle-node bifurcation: for fixed g with $g > g^*$, the equilibria e_+ and e_- undergo a saddle-node bifurcation when $I = I_{SN}(g)$ if $I \neq I_{AH}(g)$.

One can compute the first Lyapunov coefficient for the Izhikevich model in the asymptotic regimes $\gamma \ll 1, \gamma \gg 1$. The results are

$$
\begin{aligned}
l_1(0) &= \frac{\sqrt{2}}{16}\frac{(z^2+\lambda_s^2+2)^{5/2}(z^2\lambda_s\lambda_w + z\lambda_s(er-v^*(0))+\lambda_w)}{\lambda_s\sqrt{(er-v^*(0))z^3\lambda_w^{3/2}}}\frac{1}{\gamma^{5/2}} \\
&\quad + \frac{3}{16}\frac{(z^2/2+\lambda_s^2+2)^3}{\lambda_s^2 z^2(er-v^*(0))\lambda_w^2}\frac{1}{\gamma^2}, \quad \gamma \to 0, \\
l_1(0) &= \frac{3}{16}\frac{\lambda_w^2}{(er-v^*(0))^6\lambda_s^2 z^2}\gamma^3 \\
&\quad + \frac{3}{2}\frac{(4(e_r-v^*(0))^2+\lambda_w^2/2+2z\lambda_s\lambda_w(er-v^*(0)))}{(er-v^*(0))^6 z^2\lambda_s^2}\gamma^2 + O(\gamma), \quad \gamma \to \infty,
\end{aligned}
$$

where $z = g - \bar{g}$. One can immediately conclude that if $g > \bar{g}$, and $e_r - v^*(0) > 0$, the Lyapunov coefficient is positive to both leading orders in both asymptotic regimes. Thus, under fairly general conditions, the bifurcation will be a subcritical bifurcation. The derivation of the Lyapunov can be found in the supplementary material (98584_01.pdf [local/web 152KB]).

From the work done in this section, we immediately have the following theorem.

Theorem 4. *The system of equations (28)–(30) undergoes an Andronov–Hopf bifurcation when*

$$
I = I_{rh} + A_2(g)\left[N(g)^2(g-\bar{g})^2 - 2M(g)N(g)(g-\bar{g})(g-g^*)\right] + O((g-\bar{g})^2).
$$

For the Izhikevich model, this bifurcation is subcritical assuming that $e_r > v^*(0)$ and $\tau_w, \tau_s \gg 1$. If $\tau_s, \tau_w \gg 1$ and the conditions of Theorems 1 and 2 are satisfied, this bifurcation corresponds to the asynchronous steady state of the population density system (11)–(13) having a pair of pure complex conjugate eigenvalues.

3.4. The Bogdanov–Takens bifurcation condition. Recall that necessary conditions for a Bogdanov–Takens bifurcation are $\det(J) = 0$ and $\mathrm{tr}(J) = 0$. Thus, from the analysis of the last two subsections, Bogdanov–Takens bifurcations (if they exist) will occur at intersection point of the curves of saddle node and Hopf bifurcations in the g, I parameter space, i.e., at values of g such that $I_{AH}(g) = I_{SN}(g)$, with $g > \max(g^*, \bar{g})$. Using the expressions for these

curves gives

$$\begin{aligned} I_{rh} - A_2(g)M(g)^2(g-g^*)^2 &= I_{rh} + A_2(g)\left[N(g)^2(g-\bar{g})^2 - 2M(g)N(g)(g-\bar{g})](g-g^*)\right], \\ 0 &= A_2(g)\left(N(g)(g-\bar{g}) - M(g)(g-g^*)\right)^2 \\ &\Updownarrow \\ 0 &= N(g)(g-\bar{g}) - M(g)(g-g^*). \end{aligned}$$

This latter equation may be simplified to a quadratic in g:

$$g^2 g^*(\gamma-1)\frac{\lambda_s^2}{2} + g\gamma - g^*.$$

Immediately one can see that a potential solution is $\gamma = 1$, $g = g^* = \bar{g}$. However, this is a single root which lies on the switching manifold. For $\gamma \neq 1$, we have the following two pairs of Bogdanov–Takens points:

$$g_{BT\pm} = \frac{2g^*}{\gamma \mp \sqrt{\gamma^2 - 2g^*\lambda_s^2(1-\gamma)}} \tag{55}$$

which yields the following leading order asymptotics provided that $1 \gg 1-\gamma \geq 0$:

$$g_{BT+} = \frac{2}{\lambda_s^2(1-\gamma)} + O(1), \tag{56}$$

$$g_{BT-} = g^* + O(1-\gamma). \tag{57}$$

Note that g_{BT+} diverges as $1-\gamma \to 0^+$ while $g_{BT-} \to g^*$, which given the previous work implies a collision of the Bogdanov–Takens equilibrium point with the switching manifold. However, we note that these are only valid provided that $\gamma^2 - 2g^*\lambda_s^2(1-\gamma) > 0$. For the parameter sets we have looked at, we have not found a Bogdanov–Takens point as this quantity is negative. Thus, we leave the analysis of the Bogdanov–Takens point and its interaction with the switching manifold for future work.

Figure 4(a) shows the smooth bifurcations for the mean field system corresponding to a network of Izhikevich neurons with the parameter values from [7]. Note that the Hopf bifurcation for both the full and reduced mean field systems corresponds closely to the onset of bursting in the actual network, as noted in [23]. For these parameter values, $\tau_w \gg \tau_s$ and no Bogdanov–Takens' points are observed. Figure 4(b) shows the smooth bifurcations for the mean field systems corresponding to a network of AdEx neurons. In all figures the bifurcation curves derived from the small s expansions, i.e., (49) and (54), are compared with curves for the full mean field model generated numerically in MATCONT [6].

4. Nonsmooth bifurcations. To study the nonsmooth bifurcations for the mean field system (18)–(20), we will use the terminology and bifurcation classification for piecewise smooth continuous systems proposed in [5]. We note that some care must be used when applying these ideas to our system. Letting $x = [s, w]^T$ and recalling the definition (22) of the switching manifold, our system may be written in the general form used by [5]:

$$\dot{x} = \begin{cases} F_1(x, I) & \text{if } H(x, I) < 0, \\ F_2(x, I) & \text{if } H(x, I) > 0, \end{cases}$$

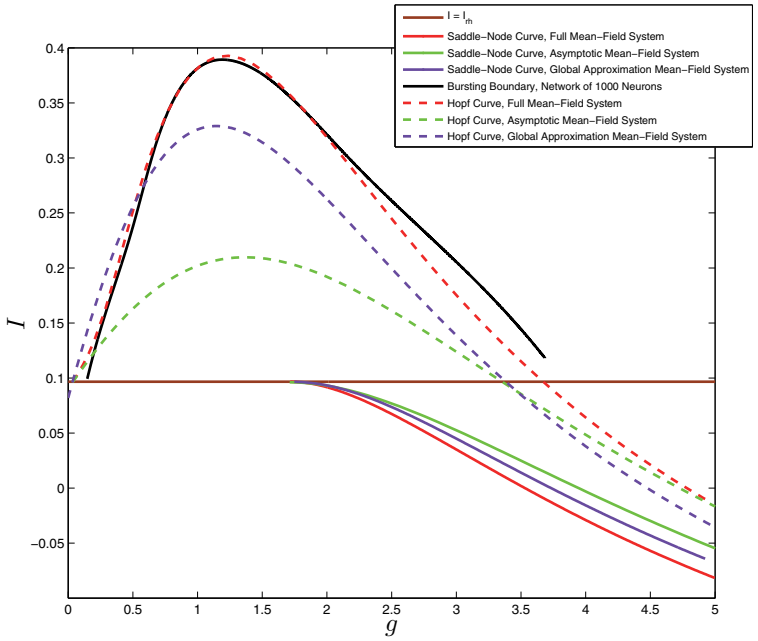

(a) Two parameter bifurcation curves, Izhikevich mean field system(s).

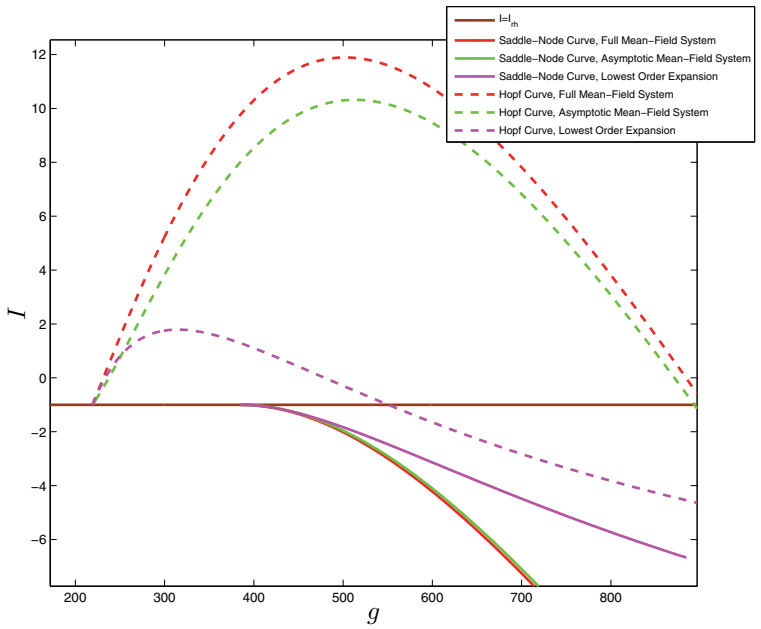

(b) Two parameter bifurcation curves, AdEx integrate and fire mean field system(s).

Figure 4. *Comparison of various approximations of the two parameter bifurcation curves for the mean field equations of the Izhikevich model* (a) *and the AdEx model* (b). *Shown are Hopf bifurcation curves (dashed lines), saddle-node bifurcation curves (dotted lines) computed for the full mean field system (red), the asymptotic mean field system (green), the lowest order approximation solution to the asymptotic mean-field system (purple), and, for the Izhikevich model, the global approximation to the mean field system (blue). For the Izhikevich model, the numerically determined bursting boundary for a network of* 1000 *neurons with the same parameters is also shown (black). The bifurcation curves for the saddle-node and Hopf bifurcations are computed using the MATLAB function* fsolve *on the determinant and trace equations of the Jacobian of the linearization. The red line corresponds to* $I = I_{rh}$.

where

$$F_1(x, I) = \begin{pmatrix} -\frac{s}{\tau_s} \\ -\frac{w}{\tau_w}, \end{pmatrix},$$

$$F_2(x, I) = F_1(x, I) + \sqrt{H(x, I)} \begin{pmatrix} \frac{\lambda_s}{\tau_s} \\ \frac{\lambda_w}{\tau_w} \end{pmatrix}.$$

However, F_2 is only defined for $H(x, I) > 0$. In contrast, the work of [5] assumes that both F_1 and F_2 are defined throughout the phase space. Nevertheless, we are able to classify a number of bifurcations in our system by analogy with the results in [5]. Additionally, due to the presence of the square root, the Jacobian diverges in the vicinity of boundary equilibrium bifurcations. This means one cannot simply unfold the system, for example, by reducing it to observer canonical form [13].

We will supplement our analysis with numerical studies of our example systems. In particular, we will perform a detailed study of the mean field system corresponding to a network of Izhikevich neurons with parameters given in Table 1.

4.1. Boundary equilibrium bifurcations ($I = I_{rh}$). Recall that all the models we are considering have an equilibrium $e_0 = (0, 0)$ which exists (and is a stable node) if $I < I^*(0, 0) = I_{rh}$. When $I = I_{rh}$, this equilibrium lies on the switching manifold $I - I^*(s, w) = 0$. When $I > I_{rh}$, this equilibrium no longer exists as the origin is not an equilibrium of the part of the mean field system corresponding to $I - I^*(w, s) > 0$. In the terminology of nonsmooth systems, the origin is a *virtual equilibrium* of the system for $I > I_{rh}$ and undergoes a *boundary equilibrium bifurcation* (BEB) when $I = I_{rh}$. The exact nature of this bifurcation depends on the value of g, in particular, its relationship to g^*, $\bar{g}$, and $\hat{g}$.

To determine the nature of the BEB, we begin by studying the nontrivial equilibria $e_\pm = (s_\pm, \eta s_\pm)$ when $I = I_{rh}$. Recalling the form (45) for $s_\pm$ and noting that $\tilde{I} = 0$ when $I = I_{rh}$, we find

$$s_+(\beta, 0) = \begin{cases} 0, & \beta < 0, \\ 2\beta, & \beta \geq 0, \end{cases}$$

$$s_-(\beta, 0) = \begin{cases} 2\beta, & \beta < 0, \\ 0, & \beta \geq 0. \end{cases}$$

Thus for $g < g^*$, e_+ collides with e_0 at $I = I_{rh}$, and for $g > g^*$, e_- collides with e_0.

Consider first the case $g^* < \bar{g}$ (which corresponds to $\tau_w < \tau_s$). In this case there is no Hopf bifurcation, so the results are straightforward. When $g < g^*$, e_+ is a sink which exists for $I > I_{rh}$. It collides with e_0 when $I = I_{rh}$ and ceases to exist when $I < I_{rh}$. Putting this together with the description of the existence and stability results for e_0, we conclude that, for this range of g values, the system undergoes a *persistence* BEB at $I = I_{rh}$. This will be either a focus/node or node/node persistence BEB depending on the classification of e_+. When $g > g^*$, recall that the equilibrium e_- is a saddle when it exists (for $I_{SN} < I < I_{rh}$). Since e_0 also exists for $I < I_{rh}$ and is a stable node, we conclude that for $g > g*$ there is a nonsmooth saddle node BEB at $I = I_{rh}$.

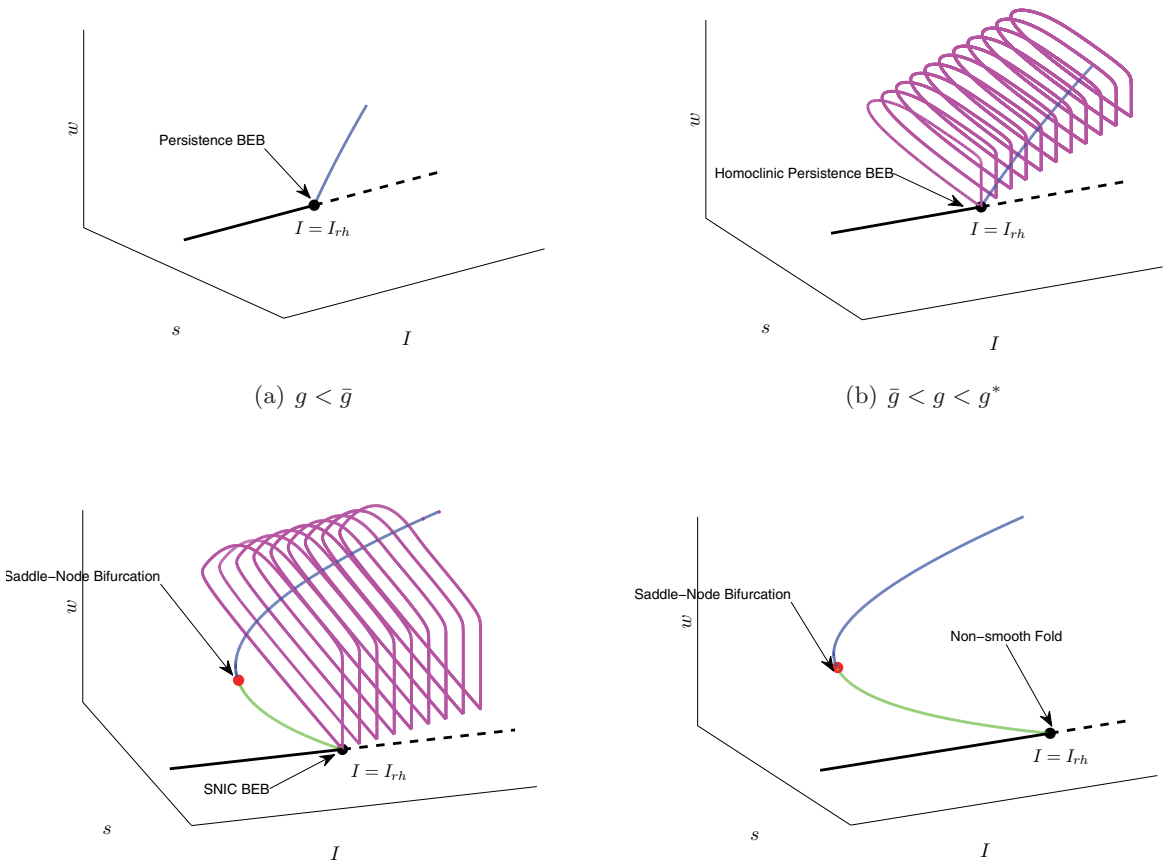

(a) $g < \bar{g}$ (b) $\bar{g} < g < g^*$

(c) $g^* < g < \hat{g}$ (d) $g \gg \hat{g}$

Figure 5. *The four branches of boundary equilibrium bifurcation (BEB) that have been found in the mean field system for the Izhikevich network. In all figures, the equilibria are e_0 (black), e_+ (blue), and e_- (green), and solid lines indicate real equilibria, while dashed lines indicate virtual ones. The magenta lines are the nonsmooth limit cycles determined via direct numerical integration.* (a) *The equilibrium e_+ collides with e_0 at $I = \frac{\alpha^2}{4}$. This results in the disappearance of e_+ for $I < \frac{\alpha^2}{4}$, while e_0 persists as a stable node. The situation is similar for* (b), *except that here the nonsmooth limit cycle collides with the BEB equilibrium point in a kind of nonsmooth homoclinic bifurcation.* (d) *The equilibrium e_- exists and is an unstable saddle for $I < \frac{\alpha^2}{4}$, as does the stable node e_0. These equilibria collide in a BEB at $I = \frac{\alpha^2}{4}$, and e_- is destroyed while e_0 becomes virtual. The bifurcation diagram in* (c) *is similar to that in* (d) *except for the emergence of a homoclinic limit cycle at the bifurcation point in a kind of nonsmooth SNIC bifurcation.*

Now consider the case $\bar{g} < g^*$. For $g < \bar{g}$, analysis similar to that above shows the system undergoes a *persistence BEB* at $I = I_{rh}$. Figure 5(a) shows this bifurcation for the mean field system corresponding to the Izhikevich network with parameters as in Table 1.

The situation for $\bar{g} < g < g^*$ is similar, except that e_+ is now an unstable focus for $I > I_{rh}$. Thus for this range of g values, there is a focus/node persistence BEB at $I = I_{rh}$. Since e_+ is a source and e_0 is a sink, we may expect (by analogy with the results in [5]) that a stable

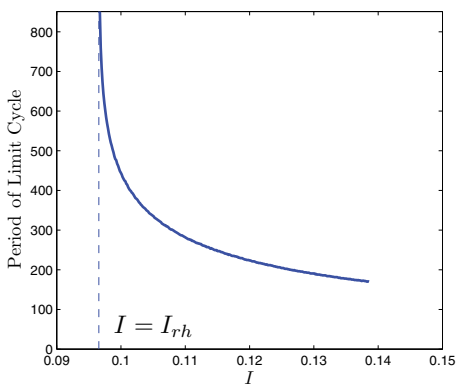

(a) Amplitude of the stable nonsmooth limit cycle.

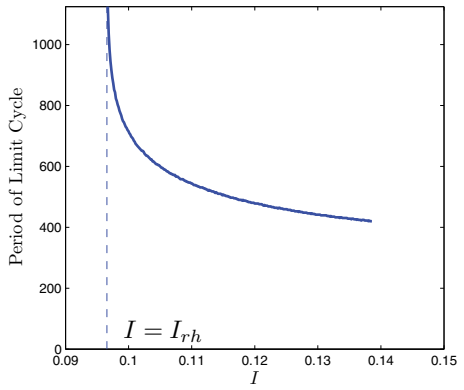

(b) Period of the stable nonsmooth limit cycle.

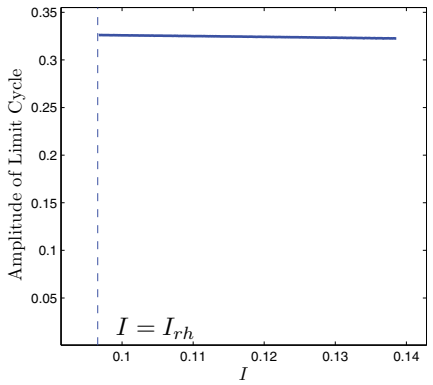

(c) Amplitude of the stable nonsmooth limit cycle.

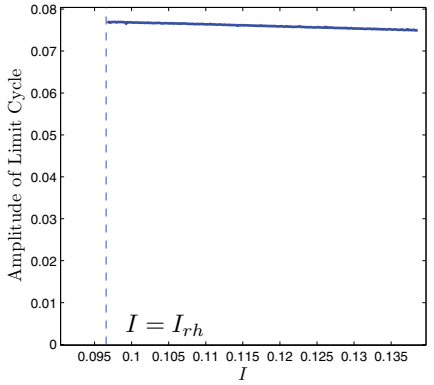

(d) Period of the stable nonsmooth limit cycle.

Figure 6. *The amplitude (*(a) *and* (c)*) and period (*(b) *and* (d)*) of the bursting limit cycle in the Izhikevich system for fixed g with $\bar{g} < g < g^*$ (left column) and $g > g^*$ (right column), respectively, as $I \to I_{rh}$. These two quantities are resolved via direct numerical simulation of the limit cycle. Note the period diverges as $I \to I_{rh}$, while the amplitude is nonzero, indicative of a homoclinic limit cycle. The amplitude is computed as the difference between the maximum and minimum w component in the steady state limit cycle.*

nonsmooth limit cycle surrounding e_+ will be created as I increases through I_{rh}. Figure 5(b) confirms this for the mean field system corresponding to the Izhikevich network. Note that in this example, the amplitude of the limit cycle does not got to zero as I approaches I_{rh}. (See also in Figure 6(c).) Further, the period of the limit cycle diverges as $I \to I_{rh}^+$. See Figure 6(a). Thus the limit cycle appears to be created in homoclinic-like bifurcation as I increases through I_{rh}. We will thus refer to this as a *homoclinic persistence BEB*.

When $g > g^*$, analysis similar to that above shows that there is a nonsmooth saddle node BEB at $I = I_{rh}$. Based on the analysis of the equilibrium points, there is no reason to expect anything more to occur with this bifurcation. However, our numerical examples show two cases. Figure 5(d) shows that a simple nonsmooth saddle-node BEB occurs for the mean field system corresponding to the Izhikevich network with $g \gg \hat{g}$. Figure 5(c) shows the bifurcation

for the same system with $g^* < g < \hat{g}$. In this case there is a nonsmooth limit cycle for $I > I_{rh}$ that appears to be destroyed when $I = I_{rh}$. Thus this bifurcation appears to be a nonsmooth version of the saddle-node on an invariant circle (SNIC) bifurcation. We will refer to it as an *SNIC BEB*. The transition between the two types of BEBs that occur for $g > g^*$ will be discussed in a later section.

Based on our numerical results we hypothesize that a nonsmooth limit cycle may be destroyed in a homoclinic-like bifurcation as I decreases through I_{rh}. We support this hypothesis in two ways.

First, consider the vector field in the neighborhood of the origin. Recall that the origin is always an attractor when it lies in the region where $H(s,w) < 0$. In the region where $H(s,w) > 0$, setting $I = I_{rh}$ and retaining only the highest order terms in s and w gives

$$\begin{aligned} s' &= -\frac{s}{\tau_s} + \frac{\lambda_s\sqrt{F''(v^*(s))}}{\tau_s}\sqrt{gs(e_r - v^*(0)) - v^{*\prime}(0)(gs)^2/2 - w} \\ &\approx \frac{\lambda_s\sqrt{F''(v^*(0))}}{\tau_s}\sqrt{gs(e_r - v^*(0)) - w}, \\ w' &= -\frac{w}{\tau_w} + \frac{\lambda_w\sqrt{F''(v^*(s))}}{\tau_w}\sqrt{gs(e_r - v^*(0)) - v^{*\prime}(0)(gs)^2/2 - w} \\ &\approx \frac{\lambda_w\sqrt{F''(v^*(0))}}{\tau_w}\sqrt{gs(e_r - v^*(0)) - w.} \end{aligned}$$

Thus, for $0 < s, w \ll 1$, and $I > I^*(s,w)$ the vector field points away from the origin and the boundary equilibrium $(0,0)$ is a repeller in this region. Since the boundary equilibrium point is as a repeller on one side of the switching manifold and an attractor on the other, it is possible for a nonsmooth homoclinic orbit to this equilibrium point to exist when $I = I_{rh}$.

Second, we show that under certain parameter conditions, if a nonsmooth limit cycle surrounds the equilibrium e_+, it must be destroyed when $I = I_{rh}$. To do this we show that trajectories that cross the switching manifold when $I = I_{rh}$ lie within the basin of attraction of the origin. Thus any nonsmooth limit cycle must become homoclinic to the origin at $I = I_{rh}$. Note that if $I - I^*(s,w) < 0$, then

$$\frac{dw}{ds} = \frac{\tau_s}{\tau_w}\frac{w}{s} = \gamma\frac{w}{s},$$

and thus $w = Cs^\gamma$ for some constant C. Assuming that the trajectory starts with (s_0, w_0) on the switching manifold, then $w = w_0\left(\frac{s}{s_0}\right)^\gamma$, where $w_0 = gs_0(e_r - v^*(0)) - v^{*\prime}(0)\frac{(gs)^2}{2}$. Now suppose this trajectory crosses the switching manifold again at (s,w). Then

$$w_0\left(\frac{s}{s_0}\right)^\gamma = gs(e_r - v^*(0)) - \frac{1}{F''(v^*(0))}\frac{(gs)^2}{2}.$$

Clearly two solutions of this equation are (s_0, w_0) and $(0,0)$. Dividing through by s and simplifying one obtains

$$(1 - ks_0)\frac{s^{\gamma-1}}{s_0^{\gamma-1}} = 1 - ks, \tag{58}$$

where $k = \frac{g}{F''(v^*(0))2(e_r - v^*(0))}$.

If $\gamma > 1$, the left-hand side of (58) is monotonically increasing while the right-hand side is a line with negative slope. Hence (s_0, w_0) is the unique intersection point. This means every trajectory that enters the region $I - I^*(s, w) < 0$ when $I = I_{rh}$ is attracted to the origin. If $\gamma < 1$, the left-hand side of (58) is now monotonically decreasing. Unless the line is tangent the curve at $(s_0, 1)$ there will always be another intersection point. Rearranging the equation shows that this intersection point will occur for $s < s_0$ if gs_0 is sufficiently small. For fixed g, this means that any trajectory that starts on the switching manifold at (w_0, s_0) with s_0 sufficiently small will be attracted to the origin. Thus all nonsmooth limit cycles that are close enough to the origin for $I > I_{rh}$ will become homoclinic to the origin when $I = I_{rh}$.

Given how $g = \bar{g}$ and $g = g^*$ delimit the different types of BEB bifurcations, it should be clear that these special points represent higher co-dimension bifurcations along the $I = I_{rh}$ line. We shall explore these bifurcations further below, in addition to determining the geometrical meaning of these points.

4.2. Saddle-node boundary equilibrium bifurcation ($I = I_{rh}, g = g^*$). From the results of the previous section, we can conclude that the point $I = I_{rh}, g = g^*$ is a special co-dimension-two bifurcation point where the boundary equilibrium bifurcation (BEB) changes from a persistence BEB to a nonsmooth saddle-node. Note that the smooth branch of saddle-node bifurcations found earlier actually emanates out from the co-dimension-two point (g^*, I_{rh}). We will show here that it does so in a highly nongeneric way as the saddle-node equilibrium hits switching manifold tangentially at the BEB, and is the only equilibrium point that interacts with the switching manifold in this way.

We have seen that regardless of the parameter values, all the nontrivial equilibria lie on the curve $w = \eta s$. Thus as any parameter is varied the nontrivial equilibrium will follow this curve, which has slope

$$w'(s) = \eta. \tag{59}$$

Further, the only equilibrium that can be a boundary equilibrium point is $e_0 = (0, 0)$, the nonfiring solution. Now the switching manifold can be written as

$$w(s) = I + F(v^*(s)) + gs(e_r - v^*(s)).$$

Thus, the slope of the switching manifold at the BEB is

$$w'(0) = g(e_r - v^*(0)). \tag{60}$$

Equating (59) and (60) shows that the nontrivial equilibrium undergoing the BEB will hit the switching manifold tangentially only if $g = g^* = \frac{\eta}{e_r - v^*(0)}$. From this it is straightforward to show that with $g = g^*$ fixed, the nontrivial equilibrium e_+ hits the switching manifold tangentially as $I \to I_{rh}$ and $s_+ \to 0$. More interesting is to consider what happens when g is varied. From our previous analysis we know that at the saddle-node bifurcation point, the saddle-node equilibrium, $e_{SN} = (s_S N(g), \eta s_S N(g))$, is defined by

$$s_{SN}(g) = M(g)(g - g^*) + O((g - g^*)^2).$$

Thus, as $g \to g^*$, $s_{SN}(g) \to 0$. This implies that the saddle-node equilibrium hits the switching manifold tangentially at $g = g^*$, $I = I_{rh}$.

In summary the point $g = g^*, I = I_{rh}$ is the collision between three branches of co-dimension-1 bifurcations: a pair of nonsmooth boundary equilibrium bifurcations and a smooth branch of saddle-node bifurcations. The details of the BEB involved depend on the relationship between g^* and $\bar{g}$. If $g^* < \bar{g}$, the BEBs are simple: a simple node/focus or focus/focus persistence BEB occurs for $g < g^*$ and a nonsmooth saddle-node BEB occurs for $g > g^*$. The case $\bar{g} < g^*$ is more complex due to the possible presence of limit cycles associated with the Hopf bifurcation. In the case we studied numerically and described in section 4.1, for $g < g^*$ we observe a homoclinic persistence BEB, and for $g > g^*$ we observe an SNIC BEB.

While this bifurcation may be complicated, the bifurcation point can be determined analytically for all the models. It is shown in detail in Figure 9(b). Of particular interest is the fact that associated with this point is a region in the $g > g^*$, $I < I_{rh}$ quadrant of the parameter space with bistability between firing and nonfiring solutions. For parameter values in the region a brief stimulus could cause the network transition from quiescence to tonic firing.

4.3. Limit cycle grazing bifurcation. The Andronov–Hopf bifurcation described in section 3.3 leads to the creation of a limit cycle. As I moves away from the bifurcation point, the amplitude of the limit cycle may increase enough that it hits the switching manifold tangentially, resulting in a grazing bifurcation. It is difficult to say much in general about the nature of this bifurcation; however, analysis similar to that in the last section shows that if $I < I_{rh}$, then once a trajectory enters the region $I - I^*(s, w) < 0$, it cannot leave, but will be attracted to the origin. Thus we expect that if a grazing bifurcation occurs for $I < I_{rh}$, it will lead to the destruction of the limit cycle.

To gain more insight, we performed a numerical study of the mean field system corresponding to the Izhikevich network with parameter values as in Table 1. We first confirmed that the Hopf bifurcation is subcritical, using MATCONT and by numerically simulating the time reversed system. Additionally, the analytically determined first Lyapunov coefficient is positive to the first two orders in the ratio of the time constants for the Izhikevich model. We then showed that the unstable limit cycle generated by the Hopf can undergo two different types of grazing bifurcations, depending on the value I. For $I > I_{rh}$, the grazing bifurcation that occurs is a persistence type grazing, i.e., the unstable limit cycle generated via the subcritical Hopf bifurcation just becomes nonsmooth after the grazing bifurcation. This is shown in Figure 7(a). Here, the limit cycle undergoes a grazing bifurcation at $I = 0.2680$, and it persists past it. Its amplitude rapidly increases past the grazing bifurcation, and it almost immediately undergoes a nonsmooth saddle-node of limit cycles with a stable nonsmooth limit cycle. For $I < I_{rh}$, the grazing bifurcation is a destruction type grazing as the limit cycle ceases to exist after the grazing for the reason discussed above. This is shown in Figure 7(b).

If the Hopf were supercritical, we would expect to see the same two types of grazing bifurcations. The only difference would be that the grazing bifurcation would occur for $I < I_{AH}$ and we would not expect the saddle-node of limit cycles bifurcation to occur.

4.4. Hopf boundary equilibrium bifurcation ($I = I_{rh}, g = \bar{g}$). The analysis of section 4.1 showed that when $\bar{g} < g^*$ the point $I = I_{rh}, g = \bar{g}$ is a co-dimension-two bifurcation

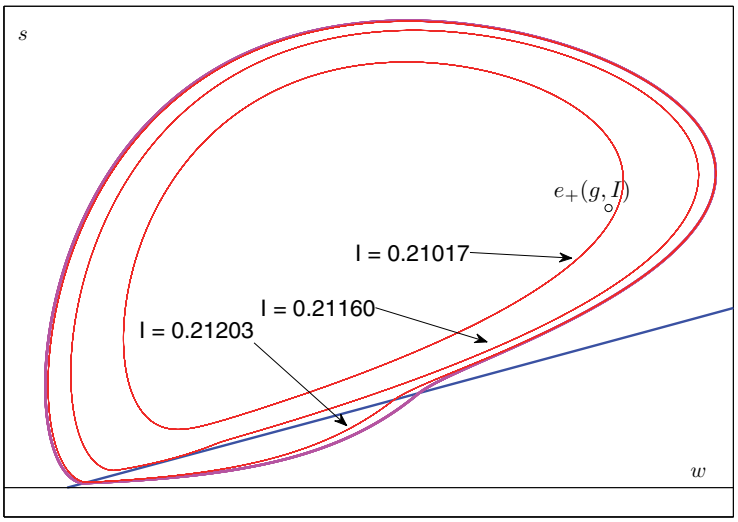

(a) Persistence grazing bifurcation and nonsmooth saddle-node of limit cycles.

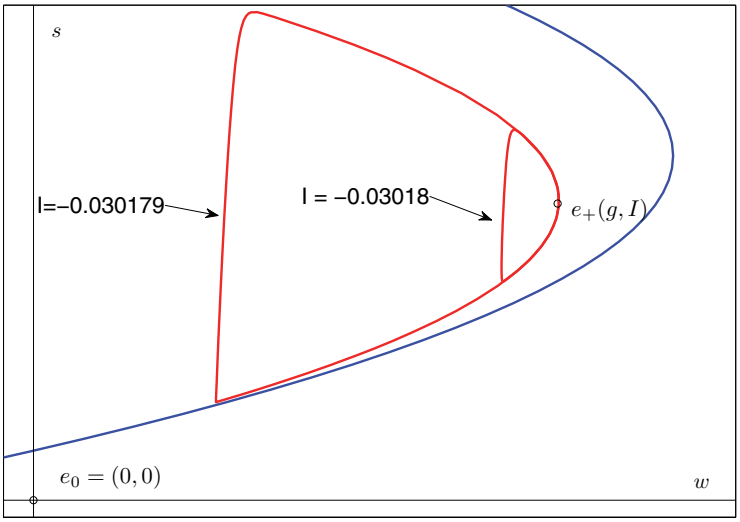

(b) Destruction grazing bifurcation.

Figure 7. *Limit cycle grazing bifurcations for the Izhikevich system.* (a) *As I is increased above $I_{AH}(g)$, for fixed g, the unstable limit cycle (shown in red) generated by the subcritical Hopf bifurcation increases in amplitude. For large enough I, the limit cycle grazes the switching manifold (shown in blue). After the grazing, the limit cycle becomes nonsmooth and subsequently collides with the nonsmooth stable limit cycle (shown in pink). The two limit cycles annihilate each other in a nonsmooth saddle node of limit cycles. Note that as I is varied, the switching manifold, the point e_+, and the unstable limit cycle all vary. However, aside from the unstable limit cycle, these other sets do not vary significantly. Thus, for clarity, we have only shown the switching manifold and stable nonsmooth limit cycle for $I = 0.2690$, and e_+ for $I = 0.2604$.* (b) *For $I < I_{rh}$ the grazing bifurcation destroys the limit cycle.*

point where the boundary equilibrium changes from a simple focus/node persistence BEB to a homoclinic persistence BEB. Recall that the two parameter Hopf bifurcation curve is given by $I = I_{AH}(g)$ as defined in section 3.3. From the analysis in that section, the equilibrium point on the Hopf curve is $e_{AH} = (s_{AH}, \eta s_{AH})$, where $s_{AH}(g) = N(g)(g - \bar{g}) + O((g - \bar{g})^2)$. Setting $I = I_{AH}(g)$ we see that as $g \to \bar{g}$, $I_{AH} \to I_{rh}$ and $e_{AH} \to e_0$, that is, the Hopf equilibrium point undergoes a BEB at $I = I_{rh}, g = \bar{g}$. We thus refer to this point as a Hopf boundary equilibrium bifurcation (Hopf BEB).

An alternative way to characterize the Hopf BEB is to fix $I = I_{rh}$ and let $g \to \bar{g}^+$. On $I = I_{rh}$, the mean field system for the Izhikevich network may be approximated as follows:

$$s' = -\frac{s}{\tau_s} + \frac{\lambda_s\sqrt{F''(v^*(s))}}{\tau_s}\sqrt{gs\Big(e_r - \frac{\alpha}{2}\Big) - \frac{(gs)^2}{4} - w} \approx \frac{\lambda_s\sqrt{F''(v^*(0))}}{\tau_s}\sqrt{gs\Big(e_r - \frac{\alpha}{2}\Big) - w},$$
$$w' = -\frac{w}{\tau_w} + \frac{\lambda_w\sqrt{F''(v^*(s))}}{\tau_w}\sqrt{gs\Big(e_r - \frac{\alpha}{2}\Big) - \frac{(gs)^2}{4} - w} \approx \frac{\lambda_w\sqrt{F''(v^*(0))}}{\tau_w}\sqrt{gs\Big(e_r - \frac{\alpha}{2}\Big) - w}$$

for (s, w) in the vicinity of the origin. Thus, we have

$$\frac{dw}{ds} = \eta\gamma + HOT$$
$$\Rightarrow w = \eta\gamma s + HOT$$

for the trajectory of the homoclinic limit cycle. Additionally, linearizing the switching manifold about the origin yields

$$w = gs\left(e_r - \frac{\alpha}{2}\right).$$

Now, using these two equations we can solve for grazing bifurcations of the homoclinic limit cycle with the switching manifold at the origin. Solving the grazing condition $w'(0) = \frac{\hat{w}}{\hat{s}} = \eta\gamma$ yields

$$g = \frac{\eta\gamma}{(e_r - \alpha/2)} = \bar{g}.$$

Thus, the Hopf BEB bifurcation can be seen as a grazing bifurcation which destroys the nonsmooth homoclinic limit cycle to the origin.

Our analysis so far shows three branches of bifurcation emanating from this co-dimension-two point: two nonsmooth BEB branches and a branch of Hopf bifurcation. As shown in Figure 5, for $g < \bar{g}$ there is a simple persistence BEB, while for $\bar{g} < g < g^*$ there is a homoclinic persistence BEB. We have numerically studied the bifurcations that occur in a neighborhood of this point for the Izhikevich model and find that that two more branches of bifurcation appear to emanate from this point as we describe below.

Let g be fixed with $g > \bar{g}$ and consider the sequence of bifurcations involving limit cycles. At $I = I_{rh}$ a stable nonsmooth limit cycle is created in a homoclinic persistence BEB, and at $I = I_{AH} > I_{rh}$ an unstable smooth limit cycle is created in a subcritical Hopf bifurcation. As I increases the smooth limit cycle becomes nonsmooth in a grazing bifurcation and then is destroyed along with the stable nonsmooth limit cycle in a saddle-node of limit cycles. We wish to determine how the grazing and saddle-node of limit cycles bifurcations behave near $g = \bar{g}$.

To do this we followed the stable nonsmooth limit cycle along the Hopf bifurcation curve. Specifically, we numerically computed the amplitude and period of the limit cycle along the curve $(g, I_{AH}(g))$ in the (g, I) parameter space with $g \to \bar{g}$. The results are shown in Figure 8, specifically Figure 8(a). The stable nonsmooth limit cycle is computed using direct simulations of the ODE system, where the system is initialized exterior to the limit cycle in the phase plane which ensures convergence. From this figure, we can see that the amplitude of the stable nonsmooth limit cycles goes to 0 as $g \to \bar{g}$. This implies that this limit cycle collapses to the origin $(0, 0)$. But as this bursting limit cycle is one part of the saddle-node of limit cycles bifurcation, then this bifurcation must also emerge from Hopf BEB. Since the grazing bifurcation lies between the saddle-node of limit cycles and the Hopf bifurcation, the persistence grazing bifurcation must also emerge from the point $g = \bar{g}, I = I_{rh}$. The entire sequence of bifurcations near the Hopf BEB is shown in Figures 9(a) and 9(d).

4.5. A co-dimension-three nonsmooth bifurcation. We briefly note that if $\tau_w = \tau_s$, then we have

$$\bar{g} = g^*, \tag{61}$$

which means that the Hopf and saddle-node BEB points coincide in a nonsmooth co-dimension-three bifurcation point. This bifurcation point may be thought of as a Bogdanov–Takens equilibrium point lying on a switching manifold. However, we note that there is no Bogdanov–Takens bifurcation (or for that matter saddle-node or Hopf bifurcations) at this point in the classical sense, as the Jacobian of the system diverges, and hence the conditions associated with these different smooth bifurcations cannot be satisfied.

This point appears to act as an organizing center for the bifurcation diagram, with all the nonsmooth bifurcations emanating from it. Due to the complexity of this point, we will leave its analysis for future work. However, it does illustrate how rich the nonsmooth bifurcation sequence of this relatively simple PWSC system is.

4.6. A global co-dimension-two nonsmooth bifurcation. In addition to the two local nonsmooth bifurcations that occur at $g = \bar{g}$, and $g = g^*$, there appears to be a global co-dimension-two bifurcation that occurs for these mean field systems. Recall that there are two different types of grazing bifurcations, a destruction type (which occurs for $I < I_{rh}$) and a persistence type (which occurs for $I > I_{rh}$). These are shown in Figure 7. Thus there is a co-dimension-two point when the grazing bifurcation crosses $I = I_{rh}$. As for the other co-dimension-two points, one may expect there would be a change in the BEB bifurcations at this point. In the case we have studied numerically it appears that the BEB changes from SNIC type before this transition to a regular nonsmooth fold after. This is shown in Figures 9(c) and 9(d). Note that this transition occurs for $g > \hat{g}$, i.e., after the second intersection of the Hopf curve with $I = I_{rh}$. It also appears that the saddle-node of nonsmooth limit cycles bifurcation emanates from this point. Note that this does not imply that there is a second impact with the Hopf equilibrium and the switching manifold, as $s_{AH}(g) = N(g)(g - \bar{g}) > 0$. This bifurcation results in the destruction of the homoclinic limit cycle that exists on $I = I_{rh}$, and it is very difficult to analyze, as it is a nonlocal co-dimension-two nonsmooth bifurcation. Geometrically, however, it occurs when the unstable smooth limit cycle (generated via the Hopf bifurcation) grazes the switching manifold at $I = I_{rh}$. If the Hopf bifurcation were

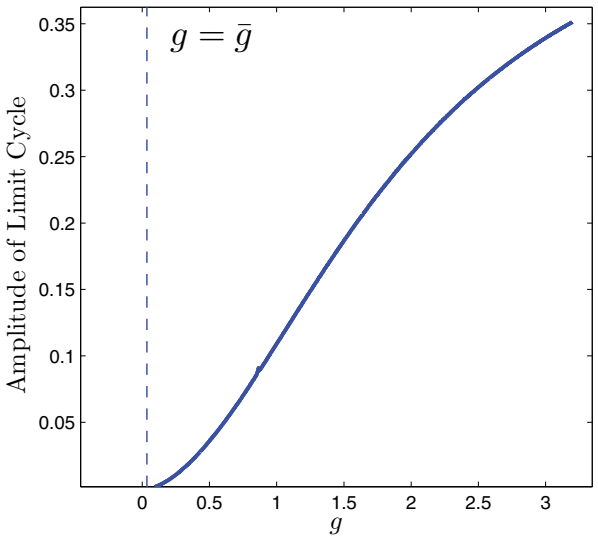

(a) Amplitude of the stable nonsmooth limit cycle.

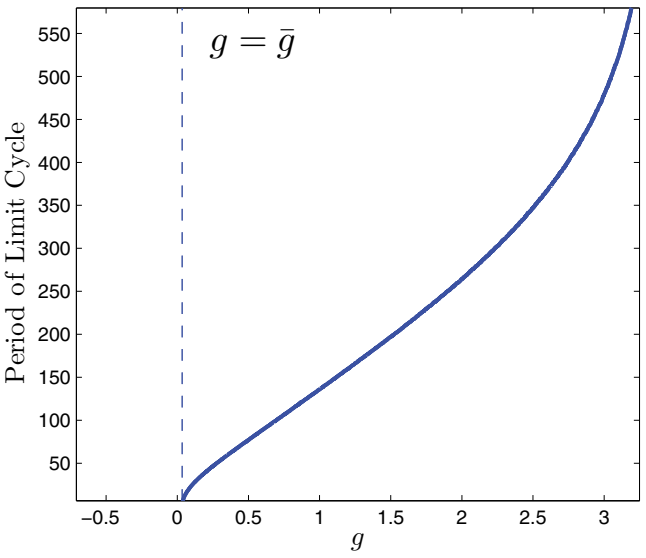

(b) Period of the stable nonsmooth limit cycle.

Figure 8. *The amplitude* (a) *and period* (b) *of the bursting limit cycle followed along the two-parameter Hopf bifurcation curve in the Izhikevich system. The Hopf bifurcation curve is entirely parameterized by g, in the (I, g) plane, and thus as we decrease g, we can compute the amplitude and period of the bursting limit cycle via direct numerical simulations. As can be seen, the amplitude decreases towards 0 as $g \to \frac{\dot{w}}{\hat{s}(e_r - \alpha/2)} = \bar{g}$, as does the period. As the bursting limit cycle is the exterior limit cycle in a nonsmooth saddle-node bifurcation of limit cycles, this bifurcation must also emanate from $\bar{g}$. Additionally, as the saddle-node of limit cycles occurs subsequent to a persistent grazing bifurcation of the unstable Hopf limit cycle, the grazing bifurcation must also emerge from this point. Also note that this is the only point in the parameter space where the homoclinic limit cycle generated does not have a divergent period as $I \to I_{rh}$. This is due to the fact that the homoclinic limit cycle has collapsed down to a point exactly at $g = \bar{g}$, and thus does not exist at this parameter value.*

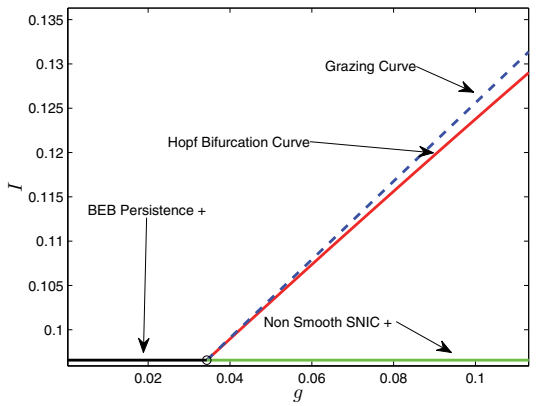

(a) Hopf BEB point (bottom left corner)).

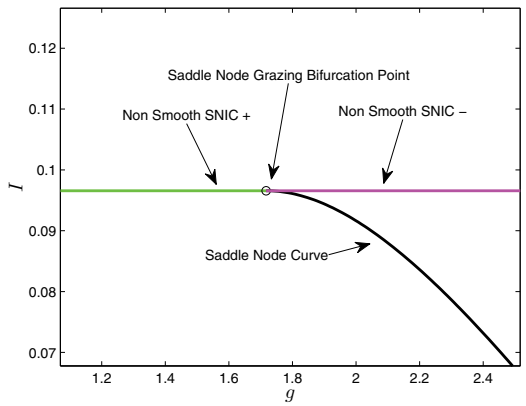

(b) Saddle-node BEB (center).

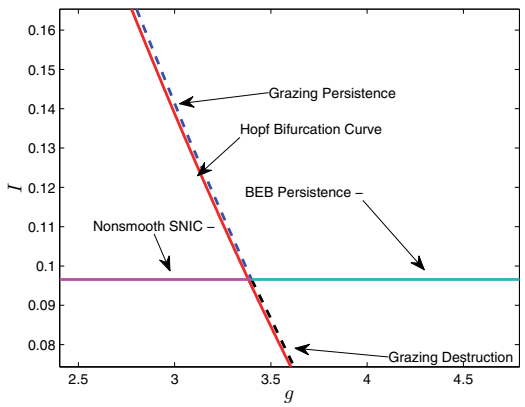

(c) Grazing alternation (bottom right corner).

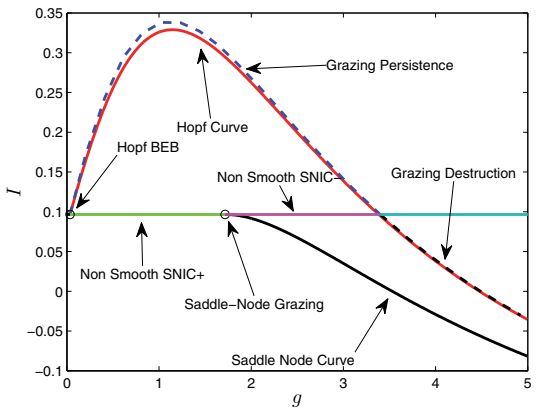

(d) Total bifurcation diagram.

Figure 9. *The entire bifurcation sequence for the Izhikevich model, including all known nonsmooth and smooth bifurcation points. Figure*(d) *is the entire diagram in the two-parameter space. Figures* (a), (b), *and* (c) *are the bottom left, center, and bottom right regions, respectively.* (a) *The co-dimension-two bifurcation point involving the collision of a branch of Hopf bifurcations with the switching manifold. This co-dimension-two point also involves a collision with a branch of grazing bifurcations of the unstable limit cycle generated by the subcritical Hopf, in addition to a branch of saddle-node of limit cycles (not shown for clarity). A nonsmooth SNIC bifurcation and BEB persistence bifurcation also collide simultaneously at the co-dimension-two point* $(\frac{\hat{w}}{\hat{s}(e_r-\alpha/2)}, \frac{\alpha^2}{4})$. (b) *The co-dimension-two saddle-node grazing point, which occurs when a saddle-node bifurcation grazes a switching manifold. The saddle-node branch of bifurcations collides at the co-dimension-two point* $(\frac{\eta}{e_r-\alpha/2}, \frac{\alpha^2}{4})$ *along with two branches of nonsmooth SNIC bifurcations.* (c) *A global co-dimension-two point. This bifurcation point involves the switching of a grazing bifurcation in the unstable Hopf limit cycle from a persistence case to a destruction case. The nonsmooth SNIC bifurcation also collides with a branch of BEB persistence bifurcations for the equilibrium* $e_-(g, I)$.

supercritical instead of subcritical, we would expect a similar co-dimension-two point to occur (if a grazing bifurcation occurred). However, it would occur for $g < \hat{g}$.

Again, due to the complexity of this particular bifurcation, further analysis is beyond the

scope of this paper, and we leave it for future work.

5. Nonsmooth bifurcations demonstrated in the network simulations. While the preceding analysis revealed a great deal of novelty and nonsmooth bifurcations for the reduced mean field system, in order for the nonsmooth analysis to be useful, it has to reflect the phenomena displayed by the actual network. Here, we will demonstrate many of the nonsmooth bifurcations predicted in the analysis are present in a full network of neurons. We will primarily consider a network of Izhikevich neurons.

A difficulty is that one cannot easily expose unstable equilibria and limit cycles in the large network of neurons using numerical simulations. For example, the equilibrium point e_- is a saddle in the mean field, and short of somehow initializing the network of neurons on the stable manifold of the saddle, it cannot be resolved via direct simulations. However, the unstable node e_+ can be resolved by modifying the network as follows. Using the separation of time scales between the fast variable s, and the slow variable w, we replace the full network (6)–(9) by the following:

$$\begin{aligned}
\dot{v}_i &= v_i(v_i-\alpha) - w_i + gs(er - v_i),\\
\dot{w}_i &= a(bv_i - w),\\
s &= \frac{\bar{w}}{\eta} = \frac{1}{\eta}\left(\frac{1}{N}\sum_{i=1}^{N} w_i\right),\\
v_i(t^-_{spike}) = v_{peak} \to & \begin{array}{rcl} v_i(t^+_{spike}) &=& v_{reset},\\ w_i(t^+_{spike}) &=& w_i(t^-_{spike}) + \hat{w}\end{array}
\end{aligned}$$

for $i = 1, 2, \ldots, N$. Here the dynamics of s are replaced entirely by its steady state, large network solution: $\lambda_s\langle R\rangle \approx w\frac{\lambda_s}{\lambda_w} = w/\eta$, with w replaced by the finite mean $\bar{w}$. We will refer to this network of neurons as the slow network.

The mean field system corresponding to the slow network is simply a one-dimensional nonsmooth ODE, given by

$$\begin{aligned}
\dot{w} &= -\frac{w}{\tau_w} + \frac{\lambda_w}{\tau_w}\langle R\rangle,\\
\langle R\rangle &= \begin{cases} \sqrt{I - I^*(w/\eta, w)}, & I \geq I^*(w/\eta, w),\\ 0, & I < I^*(w/\eta, w).\end{cases}
\end{aligned}$$

The mean field system for the slow network has the same steady states as the mean field system for the full network: the two firing solutions, $w_\pm$, and the nonfiring solution, $w_0 = 0$, with regions of existence as for the full network (see Figure 3). However, being a one-dimensional system, no Hopf bifurcations (and thus oscillations) are present in the mean field system for the slow network. Clearly, the nonfiring solution w_0 is always stable where it exists. The stability of the firing solutions is determined by the eigenvalue

$$\lambda(w_\pm) = -\frac{\lambda_w^2}{\tau_w}A_2(g)\left(1 - \frac{M(g)(g-g^*)}{M(g)(g-g^*) \pm \sqrt{M(g)^2(g-g^*)^2 + \tilde{I}}}\right), \tag{62}$$

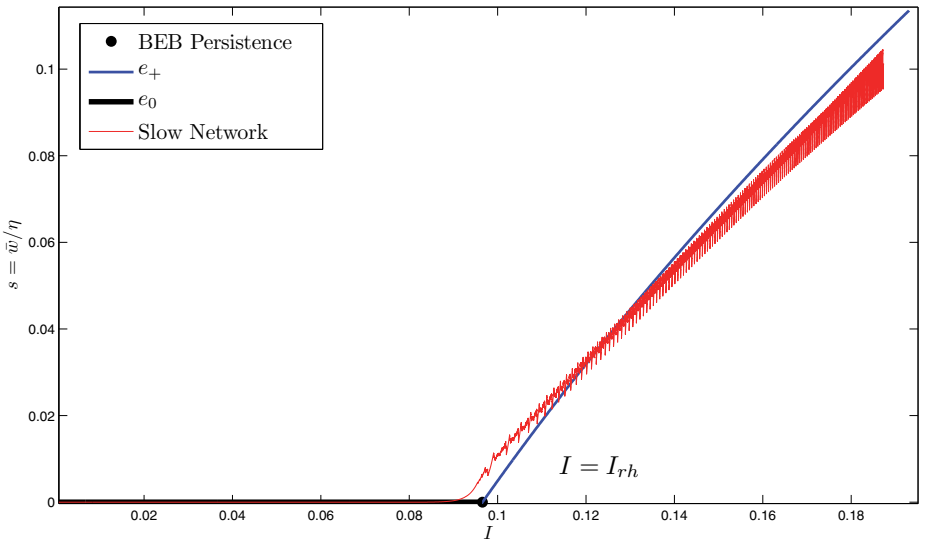

(a) $g = g^* - 1$.

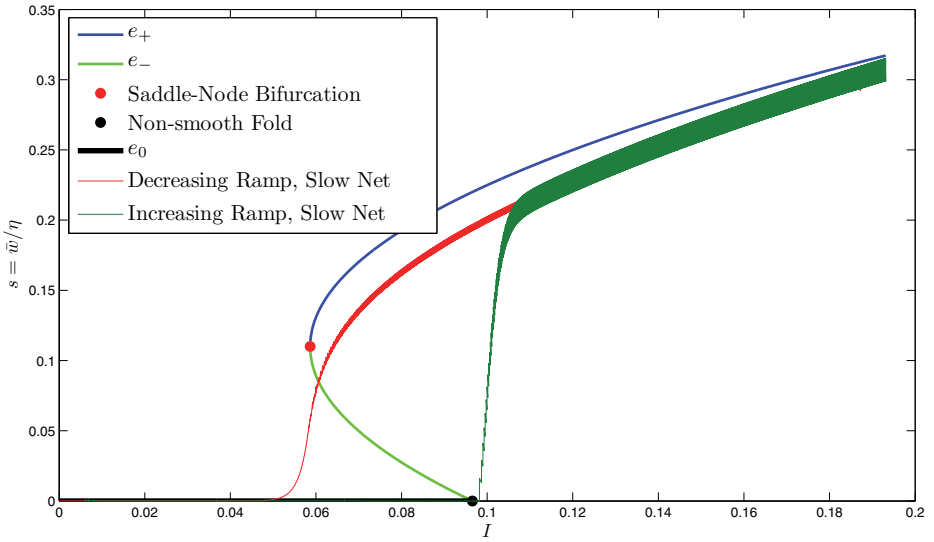

(b) $g = g^* + 1$.

Figure 10. *Comparison of the predictions of the mean field analysis and numerical simulations of a* 100*-neuron slow network with a slow current ramp for the Izhikevich system. The current is either descending (red) or ascending (green).* (a) *When $g < g^*$, as I is decreased the steady state solution for the network collides with the nonfiring solution, as predicted by the mean field analysis.* (b) *When $g > g^*$, the descending current results in firing for $I < I_{rh}$, until the steady state falls off sharply near $I = I_{SN}$. The ascending current only results in firing when $I = I_{rh}$ is reached. This behavior agrees with the mean field analysis which predicts there is bistability between these two stable states, with an unstable steady state separating them.*

where the functions $A_2(g)$ and $M(g)$ are identical to those for the mean field system for the full network. It follows that w_+ is always stable and w_- is always unstable where they exist, and that they undergo saddle-node bifurcation at $I = I_{SN}$, as for the full network. In summary, we should expect bistability between w_+ and w_0 for $I_{SN} < I < I_{rh}$, but at most one stable state elsewhere in the parameter space. Indeed, if we simulate the slow network with a slowly varying current that either decreases from current values greater than I_{rh} or increases from current values less than I_{rh}, we get bistability for $g > g^*$ and none for $g < g^*$. This is shown in Figure 10.

Using the simulations of the slow network and the full network, we can piece together a pseudobifurcation diagram for the full network. This is shown in Figure 11. The boundary equilibrium bifurcations that occur near the vicinity of g^* are also observed in the actual network. Given the similarities between the bifurcation diagram for the actual network, and that predicted by the nonsmooth mean field equations, it would appear that in order to understand the bifurcations that occur in these networks, one has to consider nonsmooth bifurcation theory.

6. Discussion. In this paper, we have made a thorough analysis of the smooth and nonsmooth bifurcations that occur in mean field systems for large networks of coupled integrate and fire neurons with spike frequency adaptation. We have shown that these systems are very rich, exhibiting global and higher co-dimension bifurcations.

Based on the analysis we have performed, there are several predictions we can make. For example, it appears that the adaptation and synaptic time scales, τ_w and τ_s, are crucial for determining the presence of bursting. If $\tau_w < \tau_s$, then no bursting can occur, while if $\tau_w > \tau_s$, there is a bell shaped region of bursting for $I > I_{rh}$, and $g > \bar{g}$. Thus, if the adaptation time scale is smaller than the time scale of the synapses, adapting, recurrently coupled networks would not burst. This can be the case, for example, for weakly adapting neurons coupled together with NMDA synapses, which have a long time scale.

One might ask whether the nonsmooth nature of the mean field system we studied is a direct result of the nonsmooth nature of the integrate and fire neural models. This is not the case. The firing rate of any type I neuron in the vicinity of the saddle-node on an invariant circle bifurcation is proportional to $\sqrt{I - I_{rh}}$. Assuming that the dynamics of the neuron voltage is much faster than the dynamics of the all the other intrinsic and synaptic currents, the mean field model for such a type I neuron should also have a square-root nonlinearity. For example, this is the case for the finite network model in the work of [10]. Thus, one has to consider nonsmooth bifurcations and bifurcation analysis when working with mean field systems for type I neurons. The same is true of type II neurons; however, the firing rate for these neurons changes discontinuously at I_{rh}, and thus it is likely that the mean field systems for type II neurons would be completely nonsmooth, as opposed to piecewise smooth continuous.

Through our analysis of the mean field systems for networks of integrate and fire neurons, we have found a number of nonsmooth bifurcations that, to the best of our knowledge, have not been previously seen in the literature. These include two co-dimension-one branches of boundary equilibrium bifurcations that have homoclinic limit cycles at the bifurcation point, and can be thought of as generating/destroying nonsmooth limit cycles. Additionally, a pair

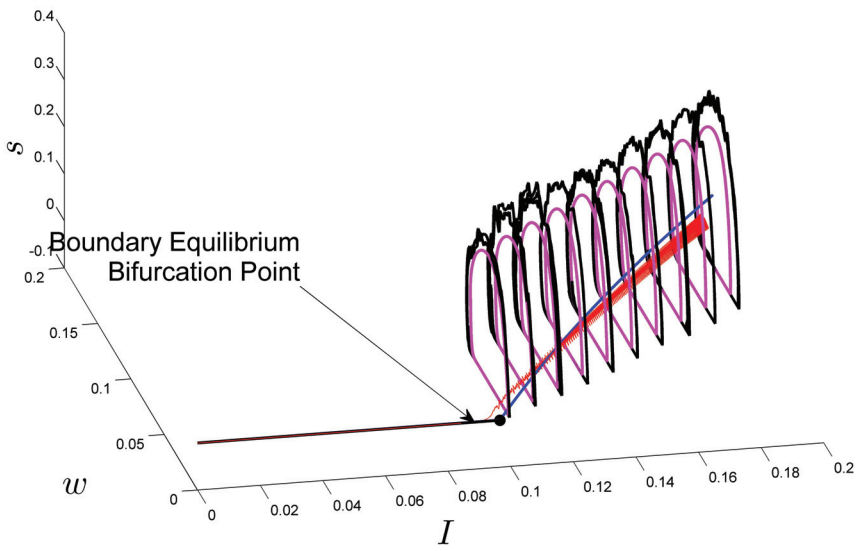

(a) $g = g^* - 1$.

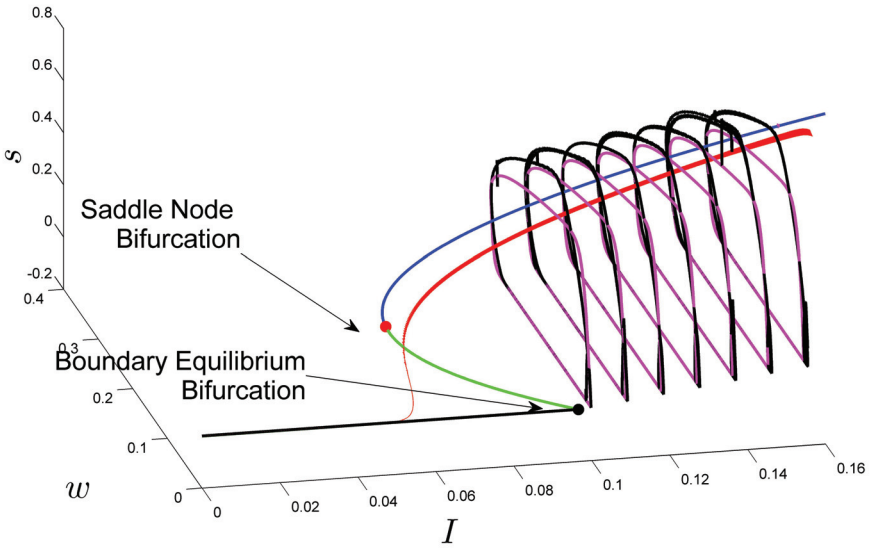

(b) $g = g^* + 1$.

Figure 11. *Using simulations of the slow network (red) to converge to the nonbursting steady state, and the full network (black) to converge to the stable bursting limit cycle, we can piece together a pseudobifurcation diagram for the full network of Izhikevich neurons that very closely mirrors the bifurcation diagram predicted from the nonsmooth mean field equations. Indeed, it appears that the transitions that occur at $I = I_{rh}$ are well explained as nonsmooth boundary equilibrium bifurcations of the mean variables of the full network. This suggests the existence of the co-dimension-two nonsmooth saddle-node BEB point for the mean variables of the actual network as well. Note that the limit cycles have been smoothed out for clarity, and some of the high frequency oscillations due to synchrony in the peaks have been removed.*

of co-dimension-two bifurcations have also been discovered that result from the collision of classical smooth branches of bifurcations with nonsmooth bifurcations. These occur when either a Hopf equilibrium point or a saddle-node equilibrium point collide with a switching manifold. We have determined locally in a neighborhood of these bifurcation points the resulting behavior of the system through analytical and numerical results. Finally, a global-codimension-two bifurcation and a nonsmooth co-dimension-three point that emerged as the collision of the two co-dimension-two points was also present.

Co-dimension-two nonsmooth bifurcations are comparatively rare in the literature for both Filippov and PWSC systems; however, some recent work has been done on both classes of systems. In particular, for PWSC systems, co-dimension-two bifurcations similar to the Hopf BEB and saddle-node BEB have been analyzed in [13, 14] while in Filippov systems co-dimension-two collisions have been analyzed in [15].

For PWSC systems, Theorems 3.1 and 3.2 in [13] analyze the collisions between saddle-node and Hopf bifurcations with persistence/nonsmooth fold bifurcations. It appears that the Hopf BEB and saddle-node BEB here correspond to nongeneric versions of the nonsmooth Hopf and nonsmooth saddle-node bifurcations in [13]. Indeed, the bifurcation sequence and properties are very similar to these other points in generic PWSC systems. The nonsmooth saddle-node bifurcation involves the intersection of a saddle-node branch at a persistence/nonsmooth fold transition. Furthermore, the branch intersects tangentially (see Figure 3.2 in [13]). The nonsmooth Hopf bifurcation in [13] has two unfoldings, with one of them being a subcritical Hopf bifurcation, followed by a limit cycle grazing and a saddle-node of limit cycles (see Figure 3.4 b in [13]). Unfortunately, due to the square root at the switching manifold present in the system we have analyzed, one cannot resort to a straightforward unfolding. The primary difference between the bifurcations present in our system and the conventional PWSC systems analyzed in [13] appears to be the homoclinic limit cycles.

Square-root systems in general have a great deal of problems with regards to straightforward applications of the existing theory. Systems in the form

$$\dot{s} = f(s,u) = -\frac{s}{\tau_s} + \frac{\lambda_s}{\tau_s}\langle R_i(t)\rangle, \tag{63}$$

$$\dot{w} = g(s,u) = -\frac{w}{\tau_w} + \frac{\lambda_w}{\tau_w}\langle R_i(t)\rangle, \tag{64}$$

$$\langle R_i(t)\rangle = \begin{cases} \sqrt{F''(v^*(s))}\sqrt{I - I^*(s,w)}, & I \geq I^*(s,w), \\ 0, & I < I^*(s,w) \end{cases} \tag{65}$$

are clearly piecewise smooth continuous. However, unlike the vast majority of PWSC systems discussed in the literature, they fail to satisfy one critical constraint that these other systems have. In normal piecewise smooth continuous systems, given by

$$\dot{x} = \begin{cases} f_1(x) & \text{if} \quad H(x) \geq 0, \\ f_2(x) & \text{if} \quad H(x) < 0, \end{cases}$$

where $f_1(x) = f_2(x)$ on $H(x) = 0$, it is assumed that both $f_1(x)$ and $f_2(x)$ exist everywhere, and are smooth. In our system, $\sqrt{I - I^*(s,w)}$ only exists when $I \geq I^*(s,w)$ and its first

derivative only exists when $I > I^*(s,w)$. This renders much of the analysis on PWSC systems inapplicable. Indeed, this system cannot even be regularized via a Teixeira type regularization scheme [3] due to the fact that $\sqrt{I - I^*(s,w)}$ is undefined when $I < I^*(s,w)$.

However, there are alternate ways to apply both center manifold theory and simultaneously regularize this system. In particular, consider the three-dimensional system given by

$$\begin{aligned}\dot{s} &= -\frac{s}{\tau_s} + \frac{\lambda_s}{\tau_s} R,\\ \dot{w} &= -\frac{w}{\tau_w} + \frac{\lambda_w}{\tau_w} R,\\ \epsilon \dot{R} &= -R\left(R^2 - F''(v^*(s))(I - I^*(s,w))\right),\end{aligned}$$

where ϵ is a small constant. In this singularly perturbed system, one can show that as $\epsilon \to 0$, one recovers the nonsmooth system (63)–(65), as when ϵ is small, we can regard s and w as fixed, and thus R rapidly converges to the steady states 0, or $\sqrt{I - I^*(s,w)}\sqrt{F''(v^*(s))}$, depending on the sign of $I - I^*(s,w)$. In particular, for ϵ sufficiently small the singularly perturbed system retains the smooth bifurcations of the nonsmooth system. However, since the singularly perturbed system is smooth, one can actually check the genericity conditions of these bifurcations. This approach can be also be thought of as a way of regularizing the nonsmooth system, by embedding it as the slow subsystem in a singular perturbation problem. Analysis of the larger smooth system can show how the nonsmooth bifurcations discovered are related to the general smooth bifurcation theory.

Using this approach, we have found that the Hopf BEB bifurcation corresponds to a Bautin point under the regularization, and the saddle-node BEB bifurcation point corresponds to a Bogdanov–Takens point under the regularization. These are both co-dimension-two smooth bifurcation, and they also explain the emergence of the nonsmooth saddle-node of periodics in the Hopf BEB, which has a smooth saddle-node of periodics. Additionally, the regularized Bogdanov–Takens has (generically) a branch of homoclinic bifurcations, which also exists in a nonsmooth form for the saddle-node BEB. However, as the singularly perturbed system and its justification as a regularization are outside of the scope of this paper, we leave it for future work.

In addition to the embedded regularization, this system is also unusual in the sense that there is a natural regularization for the mean field system. Suppose we consider the voltage equations to be perturbed by white noise:

$$\dot{v}_i = v_i(v_i - \alpha) - w_i + gs(er - v_i) + I + \eta_i, \tag{66}$$

where $\langle \eta_i(t) \rangle = 0$ and $\langle \eta_i(t)\eta_i(t') \rangle = \sigma^2 \delta(t - t')$. In this case one can rigorously derive a mean field system for this network of equations which is identical to the original mean field system given in (18)–(20) only the firing rate is now given by

$$\langle R \rangle = \left[\int_{v_{reset}}^{v_{peak}} \int_{v'}^{v_{peak}} \exp\left(-\frac{2}{\sigma^2} (M(v', w, s) - M(v, w, s)\right) dv' dv \right]^{-1}, \tag{67}$$

where $M(v,w,s)$ is an antiderivative (in v) of $F(v) - w + gs(er - v) + I$. As we shall do in forthcoming work [22] one can rigorously show that this expression for $\langle R \rangle$ is smooth with

respect to s and w, and always defined, and converges to (20) as $\sigma \to 0$. Thus, the mean field system for a network with noise parameterized by σ^2, the variance in the noise, converges to the system (18)–(20) as the variance of the noise becomes negligible. But, since the mean field system with noise is smooth, it can be thought of as a natural regularization for the nonsmooth mean field system. We remark that this is unusual in the field of nonsmooth theory as generally a regularization is chosen or suggested, and is typically of the Teixeira form [3]. We leave the bifurcation analysis of the system with noise for future work.

Finally, one may ask whether the nonsmooth bifurcations we analyze here appear in other nonsmooth systems or are generic in any way. To the best of our knowledge, the co-dimension-two bifurcations are novel in the literature, according to a recent review [4]. However, a Hopf-bifurcation occurring on a discontinuity boundary (a co-dimension-two nonsmooth bifurcation) does occur in the example (in section 6) in [20] (see Figure 29). However, the system examined in [20] is a Filippov system, and thus has a higher order of discontinuity.

Appendix A. Proof of Theorem 1.

In this section, we will show that the firing rate

$$\langle R_i(t)\rangle = \left(\int_{v_{reset}}^{v_{peak}} \frac{dv}{F(v) - w + gs(e_r - v) + I}\right)^{-1}$$

has a simple asymptotic expansion as $I - I^*(s,w) \to 0$, where I^* was defined by

$$I - I^*(s,w) = \min_v \{F(v) - w + gs(e_r - v) + I\}.$$

To prove this, we will effectively be applying Laplace's method/the saddle-point approximation. However, as the reciprocal of the firing rate is not specifically a Laplace type integral, we will have to proceed in a more direct and lengthy fashion. One can also prove this more compactly by assuming the topological equivalence of the quadratic integrate and fire neuron and a more general model in the vicinity of a saddle-node bifurcation with bifurcation parameter $I - I^*(s,w)$ [11].

Consider the reciprocal of the firing rate

$$\begin{aligned}\frac{1}{\langle R_i(t)\rangle} &= \int_{v_{reset}}^{v_{peak}} \frac{dv}{F(v) - w + gs(er - v) + I} \\ &= \int_{v_{reset}}^{v_{peak}} \frac{dv}{I - I^*(s,w) + \frac{F''(v^*)}{2}(v - v^*)^2 + \sum_{n=3}^{\infty} \frac{F^{(n)}(v^*)}{n!}(v - v^*)^n}.\end{aligned}$$

To proceed further, we will make a very particular substitution. Let $\kappa = I - I^*(s,w)$. Then the substitution

$$z = \frac{v - v^*}{\sqrt{\kappa}}, \quad dz = \frac{dv}{\sqrt{\kappa}}$$

yields the following:

$$\frac{1}{\langle R_i(t)\rangle} = \int_{(v_{reset}-v^*)/\sqrt{\kappa}}^{(v_{peak}-v^*)/\sqrt{\kappa}} \frac{\sqrt{\kappa}}{\kappa + \frac{F''(v^*)}{2}z^2\kappa + \sum_{n=1}^{\infty} \frac{F^{n+2}(v^*)}{(n+2)!}(z\sqrt{\kappa})^{n+2}}\, dz \tag{68}$$

$$= \frac{1}{\sqrt{\kappa}} \int_{(v_{reset}-v^*)/\sqrt{\kappa}}^{(v_{peak}-v^*)/\sqrt{\kappa}} \frac{1}{1 + \frac{F''(v^*)}{2}z^2} \frac{1}{\left(1 + \frac{\sum_{n=1}^{\infty} \frac{F^{n+2}(v^*)}{(n+2)!}z^{n+2}(\sqrt{\kappa})^n}{1 + \frac{F''(v^*)}{2}z^2}\right)}\, dz. \tag{69}$$

Our next step will be to expand out the second term as a geometric series, but for that we require

$$\left|\sum_{n=1}^{\infty}\frac{F^{n+2}(v^*)}{(n+2)!}z^{n+2}(\sqrt{\kappa})^n\right| \leq 1+\frac{F''(v^*)}{2}z^2. \tag{70}$$

For this to be true, we have to restrict the size of $|z|$. The reason for this is that the domain of integration is growing like $1/\sqrt{\kappa}$. It is clear that if $|z| \ll 1$, the condition (70) holds by default as the leading order term on the left-hand side is z^3, while the right-hand side is $O(1)$. For large $|z|$, in particular for $|z| = O(1/\sqrt{\kappa})$, we have another requirement that must hold. Let $M = \max\{|v_{peak}-v^*|, |v_{reset}-v^*|\}$, and $0<\zeta<1$, and assume $\zeta M/\sqrt{\kappa} < |z| < M/\sqrt{\kappa}$. Then condition (70) is satisfied provided that

$$\sum_{n=1}^{\infty}\frac{|F^{n+2}(v^*)|}{(n+2)!}\left(\frac{M}{\sqrt{\kappa}}\right)^{n+2}(\sqrt{\kappa})^n \leq 1+\zeta^2\frac{F''(v^*)}{2!}\frac{M^2}{\kappa}, \tag{71}$$

$$\frac{1}{\kappa}\sum_{n=1}^{\infty}\frac{|F^{n+2}(v^*)|}{(n+2)!}M^{n+2} \leq 1+\zeta^2\frac{F''(v^*)}{2!}\frac{M^2}{\kappa}. \tag{72}$$

Now, the dominant terms in the inequality are $O(\kappa^{-1})$ as $\kappa \ll 1$. This immediately implies that we require the following to hold:

$$\sum_{n=1}^{\infty}\frac{|F^{n+2}(v^*)|}{(n+2)!}M^n \leq \zeta^2\frac{F''(v^*)}{2!}. \tag{73}$$

Now, as the left-hand side is a function of M, it can be made sufficiently small to satisfy the inequality. Additionally, the series on the left is convergent assuming that $F(v)$ is analytic at v^*. In summary, if the second derivative dominates in a suitably small neighborhood with a width of M around v^*, the geometric series is convergent. For the neural models we are considering, this translates to the condition that if v_{peak} and v_{reset} are suitably close to v^*, the threshold for firing, and if the second derivative of F is suitably dominant, then the asymptotic expansion we will derive for the firing rate applies.

Returning to our original integral:

$$\begin{aligned}
&\frac{1}{\langle R_i(t)\rangle} \\
&= \frac{1}{\sqrt{\kappa}}\int_{(v_{reset}-v^*)/\sqrt{\kappa}}^{(v_{peak}-v^*)/\sqrt{\kappa}} \frac{1}{1+\frac{F''(v^*)}{2}z^2}\frac{1}{\left(1+\frac{\sum_{n=1}^{\infty}\frac{F^{n+2}(v^*)}{(n+2)!}z^{n+2}(\sqrt{\kappa})^n}{1+\frac{F''(v^*)}{2}z^2}\right)}\,dz \stackrel{def}{=} \frac{1}{\mathcal{R}(\kappa)} \qquad (74)\\
&= \frac{1}{\sqrt{\kappa}}\int_{(v_{reset}-v^*)/\sqrt{\kappa}}^{(v_{peak}-v^*)/\sqrt{\kappa}} \frac{1}{1+\frac{F''(v^*)}{2}z^2}\left(1-\frac{\sum_{n=1}^{\infty}\frac{F^{n+2}(v^*)}{(n+2)!}z^{n+2}(\sqrt{\kappa})^n}{(1+\frac{F''(v^*)}{2}z^2)}+HOT\right)dz \qquad (75)\\
&= \frac{1}{\sqrt{\kappa}}\int_{(v_{reset}-v^*)/\sqrt{\kappa}}^{(v_{peak}-v^*)/\sqrt{\kappa}} \frac{dz}{1+\frac{F''(v^*)}{2}z^2} - \frac{1}{\sqrt{\kappa}}\sum_{n=1}^{\infty}\int_{(v_{reset}-v^*)/\sqrt{\kappa}}^{(v_{peak}-v^*)/\sqrt{\kappa}} \frac{F^{(n+2)}(v^*)z^{n+2}(\sqrt{\kappa})^n}{(n+2)!(1+\frac{F''(v^*)}{2}z^2)^2}\,dz \\
&\quad + HOT,
\end{aligned}$$

where HOT denotes higher order terms. Note that both the first and second terms contain integrals with divergent boundaries. We will denote the first term by $1/\langle R_0\rangle = 1/\phi_0(\kappa)$, where $\phi_0(\kappa)$ will be used as a gauge function later on in our asymptotic analysis and is merely the firing rate for a type I normal form. The second term, however, is the first term in the asymptotic sequence and we need to show that it is $O(1)$. If this is the case, then $\frac{1}{\mathcal{R}(\kappa)}$ diverges as $\kappa \to 0$ as the first term diverges, and the next highest order term in the expansion is $O(1)$. More formally, if we show that the next highest order term is $O(1)$, then we have

$$\lim_{\kappa\to 0}\mathcal{R}(\kappa) = \lim_{\kappa\to 0}\left(\frac{1}{\sqrt{\kappa}}\int_{(v_{reset}-v^*)/\sqrt{\kappa}}^{(v_{peak}-v^*)/\sqrt{\kappa}} \frac{dz}{1+\frac{F''(v^*)}{2}z^2+\sum_{n=1}^{\infty}\frac{F^{n+2}(v^*)}{(n+2)!}z^{n+2}\sqrt{\kappa}^n}\right)^{-1} = 0.$$

The sum of integrals contains integrands that are functions of the form

$$\frac{z^m}{(1+az^2)^2}, \quad m = 3\ldots,$$

with a divergent boundary. Now, we'll need to analyze two cases, $m = 3$ and $m > 3$. For $m = 3$, we have the following:

$$\begin{aligned}&\int \frac{F'''(v^*)}{3!}\frac{z^3}{(1+\frac{F''(v^*)}{2}z^2)^2}\\ &= \frac{F'''(v^*)}{3!}\left(\frac{4}{2F''(v^*)^2(z^2F''(v^*)^2+4)}+\frac{2}{F''(v^*)}\log\left(1+\frac{F''(v^*)}{2}z^2\right)\right),\end{aligned} \tag{76}$$

which yields the following when evaluated with the region of integration:

$$\begin{aligned}&= \frac{F'''(v^*)}{3!}\left(\frac{4\kappa}{2F''(v^*)^2((v_{peak}-v^*)^2F''(v^*)^2+4\kappa)}-\frac{4\kappa}{2F''(v^*)^2((v_{reset}-v^*)^2F''(v^*)^2+4\kappa)}\right)\\ &+\frac{F'''(v^*)}{3!}\left(\frac{2}{F''(v^*)}\left[\log\left(1+\frac{F''(v^*)}{2\kappa}(v_{peak}-v^*)^2\right)-\log\left(1+\frac{F''(v^*)}{2\kappa}(v_{reset}-v^*)^2\right)\right]\right)\\ &= O(\kappa)+\frac{F'''(v^*)}{3!}\frac{2}{F''(v^*)}\log\left(\frac{2\kappa+F''(v^*)(v_{peak}-v^*)^2}{2\kappa+F''(v^*)(v_{reset}-v^*)^2}\right) = O(\kappa)+O(1).\end{aligned}$$

Thus, the dominant term is $O(1)$. For $m > 3$, we have

$$\frac{1}{\sqrt{\kappa}}\int_{(v_{reset}-v^*)/\sqrt{\kappa}}^{(v_{peak}-v^*)/\sqrt{\kappa}}\frac{F^{(n+2)}(v^*)z^{n+2}(\sqrt{\kappa})^n}{(n+2)!(1+\frac{F''(v^*)}{2}z^2)^2}\,dz, \quad n > 2. \tag{77}$$

The reason why we have a critical split is because for $m \geq 4$, the numerator overpowers the

denominator on a region of integration that diverges. However, the integral is in fact bounded:

$$\begin{aligned}
&\left|\frac{1}{\sqrt{\kappa}}\int_{(v_{reset}-v^*)/\sqrt{\kappa}}^{(v_{peak}-v^*)/\sqrt{\kappa}} \frac{F^{(n+2)}(v^*)z^{n+2}(\sqrt{\kappa})^n}{(n+2)!(1+\frac{F''(v^*)}{2}z^2)^2}\,dz\right| \\
&\le \frac{1}{\sqrt{\kappa}}\int_{(v_{reset}-v^*)/\sqrt{\kappa}}^{(v_{peak}-v^*)/\sqrt{\kappa}} \frac{|F^{(n+2)}(v^*)||z|^{n+2}(\sqrt{\kappa})^n}{(n+2)!(1+\frac{F''(v^*)}{2}z^2)^2}\,dz \\
&\le \frac{2}{\sqrt{\kappa}}\int_0^{M/\sqrt{\kappa}} \frac{|F^{(n+2)}(v^*)|z^{n+2}(\sqrt{\kappa})^n}{(n+2)!(1+\frac{F''(v^*)}{2}z^2)^2}\,dz \\
&\le \frac{2}{\sqrt{\kappa}}\int_0^{M/\sqrt{\kappa}} 4\frac{|F^{(n+2)}(v^*)|z^{n+2}(\sqrt{\kappa})^n}{(n+2)!(F''(v^*)z^2)^2}\,dz \qquad (78)\\
&= \frac{8}{\sqrt{\kappa}}\int_0^{M/\sqrt{\kappa}} \frac{|F^{(n+2)}(v^*)|z^{n-2}\sqrt{\kappa}^n}{(n+2)!F''(v^*)^2}\,dz \qquad (79)\\
&= \frac{8}{\sqrt{\kappa}}\frac{F^{(n+2)}(v^*)\sqrt{\kappa}^n}{(n+2)!(n-1)F''(v^*)^2}\frac{M^{n-1}}{\sqrt{\kappa}^{n-1}} \qquad (80)\\
&= 8\frac{F^{(n+2)}(v^*)M^{n-1}}{(n+2)!(n-1)F''(v^*)^2}. \qquad (81)
\end{aligned}$$

Finally, putting it all together we have

$$\begin{aligned}
&\left|\frac{1}{\sqrt{\kappa}}\sum_{n=1}^{\infty}\int_{(v_{reset}-v^*)/\sqrt{\kappa}}^{(v_{peak}-v^*)/\sqrt{\kappa}} \frac{F^{(n+2)}(v^*)z^{n+2}(\sqrt{\kappa})^n}{(n+2)!(1+\frac{F''(v^*)}{2}z^2)^2}\,dz\right| \\
&\le \left|\frac{2!F'''(v^*)}{3!F''(v^*)}\log\left(\frac{2\kappa+F''(v^*)(v_{peak}-v^*)^2}{2\kappa+F''(v^*)(v_{reset}-v^*)^2}\right)\right| \\
&\quad + O(\kappa) + \frac{2}{F''(v^*)^2}\sum_{n=2}^{\infty}\frac{F^{(n+2)}(v^*)M^{n-1}}{(n+2)!(n-1)}, \qquad (82)
\end{aligned}$$

which, under generic assumptions about the growth of the magnitude of $F^{(n+2)}(v^*)$, we know the last term converges for sufficiently small M. Thus, we have

$$\lim_{\kappa\to 0}\mathcal{R}(\kappa) = \lim_{I-I^*(s,w)\to 0^+}\langle R_i(t)\rangle = 0.$$

To simplify the asymptotic argument, let

$$K = \frac{2}{F''(v^*)^2}\sum_{n=2}^{\infty}\frac{F^{(n+2)}(v^*)M^{n-1}}{(n+2)!(n-1)} + \left|\frac{2!F'''(v^*)}{3!F''(v^*)}\log\left(\frac{F''(v^*)(v_{peak}-v^*)^2}{F''(v^*)(v_{reset}-v^*)^2}\right)\right|;$$

that is, K is all the $O(1)$ components in (82) which is the leading order term. We define our gauge function $\phi_0(\kappa)$ as

$$\phi_0(\kappa) = \left[\frac{1}{\sqrt{\kappa}}\int_{(v_{reset}-v^*)/\sqrt{\kappa}}^{(v_{peak}-v^*)/\sqrt{\kappa}}\frac{dz}{1+\frac{F''(v^*)}{2}z^2}\right]^{-1} = \sqrt{\kappa}\left[\int_{(v_{reset}-v^*)/\sqrt{\kappa}}^{(v_{peak}-v^*)/\sqrt{\kappa}}\frac{dz}{1+\frac{F''(v^*)}{2}z^2}\right]^{-1}$$

and recall $\mathcal{R}(\kappa) = \langle R_i(t) \rangle$. Then we have

$$|\mathcal{R}(\kappa) - \phi_0(\kappa)| = |\mathcal{R}(\kappa)||\phi_0(\kappa)| \left| \frac{1}{\sqrt{\kappa}} \int_{(v_{reset}-v^*)/\sqrt{\kappa}}^{(v_{peak}-v^*)/\sqrt{\kappa}} \frac{\sum_{n=1}^{\infty} \frac{F^{n+2}(v^*)}{(n+2)!}(z\sqrt{\kappa})^n dz}{\left(1 + \frac{F''(v^*)}{2} z^2\right)^2} + HOT \right|$$

$$\leq |\mathcal{R}(\kappa)|\phi_0(\kappa)| \, |K + HOT| \, . \tag{83}$$

From (83), we immediately have

$$\lim_{\kappa \to 0} \frac{|\mathcal{R}(\kappa) - \phi_0(\kappa)|}{|\phi_0(\kappa)|} \leq \lim_{\kappa \to 0} |\mathcal{R}(\kappa)|(K + HOT) = 0. \tag{84}$$

But if we explicitly integrate our gauge function we have the following:

$$\phi_0(\kappa) = \sqrt{\frac{F''(v^*)\kappa}{2}} \frac{1}{\arctan\left((v_{peak} - v^*)\sqrt{\frac{F''(v^*)}{2\kappa}}\right) - \arctan\left((v_{reset} - v^*)\sqrt{\frac{F''(v^*)}{2\kappa}}\right)} \tag{85}$$

$$\sim \frac{1}{\sqrt{2}\pi} \sqrt{F''(v^*)\kappa} + O(\kappa) \tag{86}$$

and this concludes the proof that

$$\langle R_i(t) \rangle \sim \frac{1}{\sqrt{2}\pi} \sqrt{F''(v^*(s))} \sqrt{I - I^*(s,w)} \quad \text{as} \quad I - I^*(s,w) \to 0.$$

Appendix B. Proof of Theorem 2. For the most part, the proof follows largely from the derivation originally in [1] and is also similar to the large time scale limit taken in [18].

The system we are considering is

$$\frac{\partial}{\partial t} \rho_V(v,t) = -\frac{\partial}{\partial v} \left[G(v,s,w) \rho_V(v,t) \right], \tag{87}$$

$$s' = -\frac{s}{\tau_s} + \frac{\lambda_s}{\tau_s} G(v_{peak}, s, w) \rho_V(v_{peak}, t), \tag{88}$$

$$w' = -\frac{w}{\tau_w} + \frac{\lambda_w}{\tau_w} G(v_{peak}, s, w) \rho_V(v_{peak}, t), \tag{89}$$

where $G(v,s,w) = F(v) - w + gs(e_r - v) + I$ and the assumptions on $F(v)$ and v^* are identical to Theorem 1. The system has steady state(s) given by

$$\rho_V(v,t) = \frac{\overline{\langle R \rangle}}{G(v,s,w)}, \tag{90}$$

$$s = \lambda_s \overline{\langle R \rangle}, \tag{91}$$

$$w = \lambda_w \overline{\langle R \rangle}, \tag{92}$$

$$\frac{1}{\overline{\langle R \rangle}} = \int_{v_{reset}}^{v_{peak}} \frac{dv}{G(v,s,w)}. \tag{93}$$

The existence of solutions to (90)–(93) is dealt with in section 3. It is somewhat easier to derive the spectral equation if we consider the PDE for the distribution function, instead of the density function. The distribution function PDE is given by

$$\frac{\partial P(v,t)}{\partial t} = -G(v,s,w)\frac{\partial P(v,t)}{\partial v} + G(v_{peak},s,w)\frac{\partial P(v,t)}{\partial v}\bigg|_{v=v_{peak}}. \tag{94}$$

Now, to simplify the steady state, we will apply the Abbott–Vreeswijk transform:

$$y = \int_{v_{reset}}^{v} \frac{\overline{\langle R\rangle}}{G(v', \lambda_s\overline{\langle R\rangle}, \lambda_w\overline{\langle R\rangle})}\, dv' = \eta(v). \tag{95}$$

This transformation is invertible provided that $G(v, \lambda_s\overline{\langle R\rangle}, \lambda_w\overline{\langle R\rangle}) > 0$ for all $v \in [v_{reset}, v_{peak}]$. That is, we are assuming we are in the tonic firing region of the parameter space. The resulting system is

$$\begin{aligned}
\frac{\partial P(y,t)}{\partial t} &= -\frac{\overline{\langle R\rangle}G(\eta^{-1}(y),s,w)}{G(\eta^{-1}(y),\lambda_s\overline{\langle R\rangle},\lambda_w\overline{\langle R\rangle})}\frac{\partial P(y,t)}{\partial y} + \frac{\overline{\langle R\rangle}G(v_{peak},s,w)}{G(v_{peak},\lambda_s\overline{\langle R\rangle},\lambda_w\overline{\langle R\rangle})}\frac{\partial P(y,t)}{\partial y}\bigg|_{y=1},\\
s' &= -\frac{s}{\tau_s} + \frac{\lambda_s}{\tau_s}\frac{\overline{\langle R\rangle}G(v_{peak},s,w)}{G(v_{peak},\lambda_s\overline{\langle R\rangle},\lambda_w\overline{\langle R\rangle})}\frac{\partial P(y,t)}{\partial y}\bigg|_{y=1},\\
w' &= -\frac{w}{\tau_w} + \frac{\lambda_w}{\tau_w}\frac{\overline{\langle R\rangle}G(v_{peak},s,w)}{G(v_{peak},\lambda_s\overline{\langle R\rangle},\lambda_w\overline{\langle R\rangle})}\frac{\partial P(y,t)}{\partial y}\bigg|_{y=1}.
\end{aligned}$$

Note that the steady state distribution function after performing the Abbott–Vreeswijk transform is merely $P(y) = y$. Now let $P(y,t) = y+\epsilon_y(y,t)$, $s(t) = \lambda_s\overline{\langle R\rangle}+\epsilon_s(t)$, $w = \lambda_w\overline{\langle R\rangle}+\epsilon_w(t)$. Then $\epsilon(1,t) = \epsilon(0,t) = 0$ for all $t > 0$ to satisfy the boundary conditions. Substituting this expansion into the equations gives

$$\begin{aligned}
\frac{\partial \epsilon_y(y,t)}{\partial t} &= -\overline{\langle R\rangle}\frac{G(\eta^{-1}(y),\lambda_s\overline{\langle R\rangle}+\epsilon_s(t),\lambda_w\overline{\langle R\rangle}+\epsilon_w(t))}{G(\eta^{-1}(y),\lambda_s\overline{\langle R\rangle},\lambda_w\overline{\langle R\rangle})}\left(\frac{\partial\epsilon_y(y,t)}{\partial y}+1\right)\\
&\quad + \frac{\overline{\langle R\rangle}G(v_{peak},\lambda_s\overline{\langle R\rangle}+\epsilon_s(t),\epsilon_w(t)+\lambda_w\overline{\langle R\rangle})}{G(v_{peak},\lambda_s\overline{\langle R\rangle},\lambda_w\overline{\langle R\rangle})}\left(\frac{\partial\epsilon_y(y,t)}{\partial y}+1\right)\bigg|_{y=1}\\
&= L_1(\epsilon_y(y,t),\epsilon_s(t),\epsilon_w(t)),
\end{aligned} \tag{96}$$

$$\begin{aligned}
\epsilon_s'(t) &= -\frac{\epsilon_s(t)}{\tau_s} + \frac{\overline{\langle R\rangle}\lambda_s}{\tau_s}\left(\frac{g\epsilon_s(t)(e_r-v_{peak})-\epsilon_w(t)}{G(v_{peak},\lambda_s\overline{\langle R\rangle},\lambda_w\overline{\langle R\rangle})}\right)\left(1+\frac{\partial\epsilon_y(y,t)}{\partial y}\bigg|_{y=1}\right)\\
&\quad + \frac{\overline{\langle R\rangle}\lambda_s}{\tau_s}\frac{\partial\epsilon_y(y,t)}{\partial y}\bigg|_{y=1} = L_2(\epsilon_y(y,t),\epsilon_s(t),\epsilon_w(t)),
\end{aligned} \tag{97}$$

$$\begin{aligned}
\epsilon_w'(t) &= -\frac{\epsilon_w(t)}{\tau_w} + \frac{\overline{\langle R\rangle}\lambda_w}{\tau_w}\left(\frac{g\epsilon_s(t)(e_r-v_{peak})-\epsilon_w(t)}{G(v_{peak},\lambda_s\overline{\langle R\rangle},\lambda_w\overline{\langle R\rangle})}\right)\left(1+\frac{\partial\epsilon_y(y,t)}{\partial y}\bigg|_{y=1}\right)\\
&\quad + \frac{\overline{\langle R\rangle}\lambda_w}{\tau_w}\frac{\partial\epsilon_y(y,t)}{\partial y}\bigg|_{y=1} = L_3(\epsilon_y(y,t),\epsilon_s(t),\epsilon_w(t)).
\end{aligned} \tag{98}$$

Note that

$$L(\epsilon_y(y,t),\epsilon_s(t),\epsilon_w(t)) = \begin{pmatrix} L_1(\epsilon_y(y,t),\epsilon_s(t),\epsilon_w(t)) \\ L_2(\epsilon_y(y,t),\epsilon_s(t),\epsilon_w(t)) \\ L_3(\epsilon_y(y,t),\epsilon_s(t),\epsilon_w(t)) \end{pmatrix}$$

is an operator on the Banach space $\Omega = \mathbb{L}_2[0,1]\times\mathbb{R}^2$. The linearization of the system (96)–(98) about $\mathbf{0}$ is determined by Frechet derivative of the operator L. It is straightforward to show that the linearization is $DL(\mathbf{0})$ defined by

$$\begin{aligned}
DL_1(0)\boldsymbol{h} &= -\overline{\langle R\rangle}\left(\frac{\partial h_1(y)}{\partial y} - \frac{\partial h_1(y)}{\partial y}\bigg|_{y=1}\right) \\
&\quad - \overline{\langle R\rangle}\left(\frac{gh_2(e_r-\eta^{-1}(y))-h_3}{G(\eta^{-1}(y),\lambda_s\overline{\langle R\rangle},\lambda_w\overline{\langle R\rangle})} - \frac{gh_2(e_r-v_{peak})-h_3}{G(v_{peak},\lambda_s\overline{\langle R\rangle},\lambda_w\overline{\langle R\rangle})}\right), \\
DL_2(0)\boldsymbol{h} &= -\frac{h_2}{\tau_s} + \frac{\overline{\langle R\rangle}\lambda_s}{\tau_s}\left(\frac{gh_2(e_r-v_{peak})-h_3}{G(v_{peak},\lambda_s\overline{\langle R\rangle},\lambda_w\overline{\langle R\rangle})}\right) + \frac{\overline{\langle R\rangle}\lambda_s}{\tau_s}\frac{\partial h_1(y)}{\partial y}\bigg|_{y=1}, \\
DL_3(0)\boldsymbol{h} &= -\frac{h_3}{\tau_w} + \frac{\overline{\langle R\rangle}\lambda_w}{\tau_w}\left(\frac{gh_2(e_r-v_{peak})-h_3}{G(v_{peak},\lambda_s\overline{\langle R\rangle},\lambda_w\overline{\langle R\rangle})}\right) + \frac{\overline{\langle R\rangle}\lambda_w}{\tau_w}\frac{\partial h_1(y)}{\partial y}\bigg|_{y=1}.
\end{aligned}$$

Now, we can proceed to determine the spectrum of eigenvalues for this linear operator, i.e., the complex numbers μ such that

$$D_L(\mathbf{0})\boldsymbol{h} = \mu\boldsymbol{h}.$$

Defining

$$A(y) = \frac{g(e_r-\eta^{-1}(y))}{G(\eta^{-1}(y),\lambda_s\overline{\langle R\rangle},\lambda_w\overline{\langle R\rangle})}, \tag{99}$$

$$B(y) = \frac{-1}{G(\eta^{-1}(y),\lambda_s\overline{\langle R\rangle},\lambda_w\overline{\langle R\rangle})}, \tag{100}$$

we can write the eigenvalue problem as

$$\mu h_1(y) = -\overline{\langle R\rangle}(h_1'(y)-h_1'(1)) - \overline{\langle R\rangle}[h_2(A(y)-A(1)) + h_3(B(y)-B(1))], \tag{101}$$

$$\mu h_2 = -\frac{h_2}{\tau_s} + \frac{\overline{\langle R\rangle}\lambda_s}{\tau_s}\left(h_2A(1)+h_3B(1)+h_1'(1)\right), \tag{102}$$

$$\mu h_3 = -\frac{h_3}{\tau_w} + \frac{\overline{\langle R\rangle}\lambda_w}{\tau_w}\left(h_2A(1)+h_3B(1)+h_1'(1)\right). \tag{103}$$

Note that the solution must satisfy the boundary conditions $h_1(0) = h_1(1) = 0$. Solving (101) for $h_1(y)$ and using $h_1(0) = 0$ yields

$$\begin{aligned}
h_1(y)e^{y\mu/\overline{\langle R\rangle}} &= \frac{\overline{\langle R\rangle}}{\mu}(e^{y\mu/\overline{\langle R\rangle}}-1)(h_1'(1)+h_2A(1)+h_3B(1)) \\
&\quad - \int_0^y e^{y'\mu/\overline{\langle R\rangle}}(h_2A(y')+h_3B(y'))\,dy'.
\end{aligned}$$

Applying the condition $h_1(1) = 0$ then determines $h_1'(1)$:

$$h_1'(1) = \frac{\mu}{\overline{\langle R\rangle}}(e^{\mu/\overline{\langle R\rangle}} - 1)^{-1} \int_0^1 e^{y'\mu/\overline{\langle R\rangle}}(h_2 A(y') + h_3 B(y'))\, dy' - h_2 A(1) - h_3 B(1).$$

This allows us to solve for the first component of the eigenfunction:

$$\begin{aligned} h_1(y) = &\left(\frac{e^{y\mu/\overline{\langle R\rangle}} - 1}{e^{\mu/\overline{\langle R\rangle}} - 1}\right) \int_0^1 e^{(y'-y)\mu/\overline{\langle R\rangle}}(h_2 A(y') + h_3 B(y'))\, dy' \\ &- \int_0^y e^{(y'-y)\mu/\overline{\langle R\rangle}}(h_2 A(y') + h_3 B(y'))\, dy'. \end{aligned}$$

Defining

$$\begin{aligned} \hat{A}(\mu) &= \int_0^1 e^{y'\mu/\overline{\langle R\rangle}} A(y')\, dy', \\ \hat{B}(\mu) &= \int_0^1 e^{y'\mu/\overline{\langle R\rangle}} B(y')\, dy', \end{aligned}$$

and using the expression for $h_1'(1)$, we have

$$\begin{aligned} h_2\left(\mu + \frac{1}{\tau_s} - \frac{\mu\lambda_s}{\tau_s(e^{\mu/\overline{\langle R\rangle}} - 1)}\hat{A}(\mu)\right) + h_3\left(\frac{-\mu\lambda_s}{\tau_s(e^{\mu/\overline{\langle R\rangle}} - 1)}\hat{B}(\mu)\right) = 0, \\ h_2\left(-\frac{\mu\lambda_w}{\tau_w(e^{\mu/\overline{\langle R\rangle}} - 1)}\hat{A}(\mu)\right) + h_3\left(\mu + \frac{1}{\tau_w} - \frac{\mu\lambda_w}{\tau_w(e^{\mu/\overline{\langle R\rangle}} - 1)}\hat{B}(\mu)\right) = 0, \end{aligned}$$

or

$$\boldsymbol{M}(\mu)\begin{pmatrix} h_2 \\ h_3 \end{pmatrix} = 0.$$

For nontrivial eigenfunctions we require $\det \boldsymbol{M}(\mu) = 0$, which yields the spectral equation:

(104)
$$\left(e^{\mu/\overline{\langle R\rangle}} - 1\right)\left(\mu + \frac{1}{\tau_s}\right)\left(\mu + \frac{1}{\tau_w}\right) - \left(\mu + \frac{1}{\tau_s}\right)\left(\frac{\lambda_w}{\tau_w}\mu\hat{B}(\mu)\right) - \left(\mu + \frac{1}{\tau_w}\right)\left(\frac{\lambda_s}{\tau_s}\mu\hat{A}(\mu)\right) = 0.$$

This determines the eigenvalues, μ, of the linear operator $Dh(\mathbf{0})$, and thus the stability of the steady state solution to (90)–(93).

Previously, we derived the mean field system of differential equations via a perturbation argument. We assumed that $\tau_w^{-1} = \epsilon$ was small, and $\tau_s = \tau_w\gamma$, where $\gamma = O(1)$. Applying the same assumptions here yields spectral equation

$$\left(e^{\mu/\overline{\langle R\rangle}} - 1\right)\left(\mu + \frac{\epsilon}{\gamma}\right)(\mu + \epsilon) - \left(\mu + \frac{\epsilon}{\gamma}\right)\epsilon\lambda_w\mu\hat{B}(\mu) - \frac{\lambda_s}{\gamma}(\mu + \epsilon)\,\epsilon\mu\hat{A} = 0.$$

We look for perturbation solutions to this system, $\mu = \mu_0 + \epsilon\mu_1$. The $O(1)$ problem is immediately resolvable:

$$\mu_0^2(\exp(\mu_0/\overline{\langle R\rangle}) - 1) = 0,$$

which has solutions $\mu_0 = 0$ with multiplicity 2, and $\mu_0 = 2n\pi_i\overline{\langle R\rangle}$. Let us first consider the $\mu_0 = 0$ solution, i.e., $\mu = \epsilon\mu_1$. Then μ_1 satisfies

$$\epsilon^3\left(\frac{\mu_1}{\overline{\langle R\rangle}} + O(\epsilon)\right)\left(\mu_1 + \gamma^{-1}\right)(\mu_1 + 1) - \epsilon^3\left(\mu_1 + \gamma^{-1}\right)\mu_1\lambda_w\hat{B}(\mu_1\epsilon) - \epsilon^3(\mu_1+1)\gamma^{-1}\lambda_s\mu_1\hat{A}(\mu_1\epsilon).$$

We need to determine the leading order behavior of

$$\hat{A}(\mu_1\epsilon) = \int_0^1 e^{\epsilon y'\mu_1/\overline{\langle R\rangle}}A(y')\,dy = \int_0^1 A(y')\,dy' + O(\epsilon), \tag{105}$$

$$\hat{B}(\mu_1\epsilon) = \int_0^1 e^{\epsilon y'\mu_1/\overline{\langle R\rangle}}B(y')\,dy = \int_0^1 B(y')\,dy' + O(\epsilon). \tag{106}$$

Undoing the substitutions we had before yields the following:

$$\int_0^1 A(y')\,dy' = \int_0^1 \frac{g(e_r - \eta^{-1}(y'))}{G(\eta^{-1}(y')\lambda_s\overline{\langle R\rangle}, \lambda_w\overline{\langle R\rangle})}\,dy' \tag{107}$$

$$= \overline{\langle R\rangle}\int_{v_{reset}}^{v_{peak}} \frac{g(e_r - v)}{G(v, \lambda_s\overline{\langle R\rangle}, \lambda_w\overline{\langle R\rangle})^2}\,dv, \tag{108}$$

$$\int_0^1 B(y')\,dy' = \int_0^1 \frac{1}{G(\eta^{-1}(y'), \lambda_s\overline{\langle R\rangle}, \lambda_w\overline{\langle R\rangle})}\,dy' \tag{109}$$

$$= \overline{\langle R\rangle}\int_{v_{reset}}^{v_{peak}} \frac{-1}{G(v, \lambda_s\overline{\langle R\rangle}, \lambda_w\overline{\langle R\rangle})^2}\,dv'. \tag{110}$$

Recalling the definition (93) of $\overline{\langle R\rangle}$ yields

$$\int_0^1 A(y')\,dy' = \frac{1}{\overline{\langle R\rangle}}\frac{\partial\langle R_i(t)\rangle}{\partial s}\bigg|_{(\lambda_s\overline{\langle R\rangle},\lambda_w\overline{\langle R\rangle})}, \tag{111}$$

$$\int_0^1 B(y')\,dy' = \frac{1}{\overline{\langle R\rangle}}\frac{\partial\langle R_i(t)\rangle}{\partial w}\bigg|_{(\lambda_s\overline{\langle R\rangle},\lambda_w\overline{\langle R\rangle})}. \tag{112}$$

Collecting all the $O(\epsilon^3)$ terms in the equation for μ_1 we have

$$\frac{\mu_1}{\overline{\langle R\rangle}}(\mu_1 + \gamma^{-1})(\mu_1+1) - \frac{\mu_1}{\overline{\langle R\rangle}}\lambda_w(\mu_1+\gamma^{-1})\frac{\partial\overline{\langle R\rangle}}{\partial w} - \gamma^{-1}\lambda_s\frac{\mu_1}{\overline{\langle R\rangle}}(\mu_1+1)\frac{\partial\overline{\langle R\rangle}}{\partial s} = 0$$

or, equivalently,

$$(\mu_1 + \gamma^{-1})(\mu_1+1) - \lambda_w(\mu_1+\gamma^{-1})\frac{\partial\overline{\langle R\rangle}}{\partial w} - \gamma^{-1}\lambda_s(\mu_1+1)\frac{\partial\overline{\langle R\rangle}}{\partial s} = 0. \tag{113}$$

The above is the characteristic polynomial for the Jacobian of the mean field system of equations given by (18)–(20) when we back substitute for $\mu_1 = \mu/\epsilon + O(\epsilon)$. Thus, we know that two solutions for μ_1 are equivalent to the mean field eigenvalues for the steady state up to $O(\epsilon)$.

Now, consider $\mu_0 = 2n\pi i\overline{\langle R\rangle}$. In this case, the $O(\epsilon)$ problem is

$$-4n^2\pi^2\mu_1\overline{\langle R\rangle} + 4n^2\pi^2\overline{\langle R\rangle}^2\lambda_w\hat{B}(2n\pi i) + 4n^2\pi^2\overline{\langle R\rangle}^2\lambda_s\gamma^{-1}\hat{A}(2n\pi i) = 0.$$

Solving gives

$$\begin{aligned}
\mu_1 &= \overline{\langle R\rangle}\lambda_w\hat{B}(2n\pi i\overline{\langle R\rangle}) + \overline{\langle R\rangle}\gamma^{-1}\lambda_s\hat{A}(2n\pi i\overline{\langle R\rangle}) \\
&= \lambda_w\overline{\langle R\rangle}\int_0^1 e^{2n\pi iy'}B(y')\,dy' + \overline{\langle R\rangle}\gamma^{-1}\lambda_s\int_0^1 e^{2n\pi iy'}A(y')\,dy' \\
&= \overline{\langle R\rangle}\gamma^{-1}\int_0^1 e^{2n\pi iy}\frac{g\lambda_s(e_r-\eta^{-1})(y)-\gamma\lambda_w}{G(\eta^{-1}(y),\lambda_s\overline{\langle R\rangle},\lambda_w\overline{\langle R\rangle})}\,dy.
\end{aligned}$$

Provided that the real components of μ_1 are negative, then the mean field system forms a stable slow manifold that the solutions of the PDE system converge to assuming that $\overline{\langle R\rangle} > 0$. Consider the case when $G(v,s,w)$ is for a network of Izhikevich/quadratic integrate and fire neurons:

$$\begin{aligned}
G(v,\lambda_s\overline{\langle R\rangle},\lambda_w\overline{\langle R\rangle}) &= I - I^*(\lambda_s\overline{\langle R\rangle},\lambda_w\overline{\langle R\rangle}) + F''(v^*)\frac{(v-v^*)^2}{2!} \\
&= \kappa + F''(v^*)\frac{(v-v^*)^2}{2!}, \\
y = \eta(v) &= \int_{v_{reset}}^{v}\frac{\overline{\langle R\rangle}dv'}{\kappa + F''(v^*)\frac{(v-v^*)^2}{2!}} \\
&= \overline{\langle R\rangle}\sqrt{\frac{2}{F''(v^*)\kappa}}\left[\arctan\left((v-v^*)\sqrt{\frac{F''(v^*)}{2\kappa}}\right)\right. \\
&\quad \left. - \arctan\left((v_{reset}-v^*)\sqrt{\frac{F''(v^*)}{2\kappa}}\right)\right], \\
v = \eta^{-1}(y) &= v^* \\
&\quad + \sqrt{\frac{2\kappa}{F''(v^*)}}\tan\left[\frac{1}{\overline{\langle R\rangle}}\sqrt{\frac{\kappa F''(v^*)}{2}}y + \arctan\left((v_{reset}-v^*)\sqrt{\frac{F''(v^*)}{2\kappa}}\right)\right] \\
&= v^* + \sqrt{\frac{2\kappa}{F''(v^*)}}\tan(Cy+D), \\
G(\eta^{-1}(y),\lambda_s\overline{\langle R\rangle},\lambda_w\overline{\langle R\rangle}) &= \kappa + \frac{F''(v^*)}{2}\frac{2\kappa}{F''(v^*)}\tan(Cy+D)^2 \\
&= \kappa(1+\tan^2(Cy+D)), \\
C &= \frac{1}{\overline{\langle R\rangle}}\sqrt{\frac{\kappa F''(v^*)}{2}} = \arctan\left((v_{peak}-v^*)\sqrt{\frac{F''(v^*)}{2\kappa}}\right) \\
&\quad + \arctan\left((v^*-v_{reset})\sqrt{\frac{F''(v^*)}{2\kappa}}\right)
\end{aligned}$$

$$\sim \pi - \sqrt{\frac{2\kappa}{F''(v^*)}}\left(\frac{1}{v_{peak}-v^*}+\frac{1}{v^*-v_{reset}}\right), \quad \kappa \to 0,$$

$$D = -\arctan\left((v^*-v_{reset})\sqrt{\frac{F''(v^*)}{2\kappa}}\right)$$

$$\sim -\frac{\pi}{2} + \sqrt{\frac{2\kappa}{F''(v^*)}}\frac{1}{v^*-v_{reset}}, \quad \kappa \to 0.$$

The sign of the real part of μ_1 can be determined by

$$\begin{aligned}\mathrm{Re}(\mu_1) &= \overline{\langle R\rangle}\gamma^{-1}\int_0^1 \frac{\cos(2n\pi y')\left(g\lambda_s\gamma\left(e_r - v^* - \sqrt{\frac{2\kappa}{F''(v^*)}}\tan(Cy'+D)\right)-\lambda_w\right)}{\kappa(1+\tan^2(Cy'+D))}\,dy' \\ &= \frac{H_1(C,D)}{\kappa}\left(\frac{g\lambda_s\gamma(e_r-v^*)-\lambda_w}{-2n^2\pi^2+2C^2}\right)+\frac{H_2(C,D)}{\sqrt{\kappa}}\left(\frac{g\gamma\lambda_s}{(-2n\pi^2+2C^2)\sqrt{F''(v^*)}}\right)\end{aligned}$$

(114)
$$\begin{aligned}H_1(C,D) &= 2C\left(\cos(C)^2\sin(D)\cos(D)+\left(\cos(D)^2-\frac{1}{2}\right)\sin(C)\cos(C)-\sin(D)\cos(D)\right) \\ H_2(C,D) &= 2\sqrt{2}C\left(\left(\cos(D)^2-\frac{1}{2}\right)\cos(C)^2-\frac{1}{4}\sin(2C)\sin(2D)-\cos(D)^2+\frac{1}{2}\right).\end{aligned}$$

Provided that $H_1(C,D)>0$, then $\mu_1<0$ if $\kappa \ll 1$ and the quantity $g(e_r-v^*(0))\lambda_s-\gamma\lambda_w = (e_r-v^*(0))\lambda_s(g-\bar{g})>0$. For the theta neuron ($v_{peak}=\infty, v_{reset}=-\infty$), when the quantities H_1 and H_2 are evaluated at $D=-\pi/2$ and $C=\pi$ one obtains $H_1=H_2=0$, and one has to compute a higher order perturbation to resolve this as the $O(\epsilon)$ contribution is 0. For all the other neuron models, however, $H_1(C,D)>0$ when $C<\pi$ and $D>-\frac{\pi}{2}$ locally near $C=\pi$ and $D=-\frac{\pi}{2}$ which is precisely the case when one expands C and D asymptotically.

This implies that for the quadratic integrate and fire neuron, with $v_{peak}<\infty$ and $v_{reset}>-\infty$, as $I-I^*(s,w)\to 0^+$, and $\tau_w,\tau_s \gg 1$, the mean field system of equations forms a finite dimensional stable slow manifold if $g>\bar{g}$. Note that to lowest order, if one replicates the asymptotic analysis of integrals in the proof of Theorem 1 for the Fourier coefficients of $A(y)$ and $B(y)$, we arrive at the same quantities for the more general neuron types (AdEx, etc.) that we have considered (to lowest order).

REFERENCES

[1] L.F. Abbott and C. van Vreeswijk, *Asynchronous states in networks of pulse-coupled oscillators*, Learning Memory, 48 (1993), pp. 1483–1490.

[2] R. Brette and W. Gerstner, *Adaptive exponential integrate-and-fire model as an effective description of neuronal activity*, J. Neurophysiol., 94 (2005), pp. 3637–3642.

[3] A. Buzzi, P.R. da Silva, and M.A. Teixeira, *A singular approach to discontinuous vector fields on the plane*, J. Differential Equations, 231 (2006), pp. 633–655.

[4] A. Colombo, M. di Bernardo, and M.R. Jeffrey, *Bifurcations of piecewise smooth flows: Perspectives, methodologies and open problems*, Phys. D, 241 (2011), pp. 1845–1860.

[5] M. di Bernardo, C.J. Budd, A.R. Champneys, P. Kowalczyk, A.B. Nordmark, G.O. Tost, and P.T. Piiroinen, *Bifurcations in nonsmooth dynamical systems*, SIAM Rev., 50 (2008), pp. 629–701.

[6] A. Dhooge, W. Govaerts, and Yu.A. Kuznetsov, *MATCONT: A MATLAB package for numerical bifurcation analysis of ODEs*, ACM Trans. Math. Software, 29 (2003), pp. 141–164.
[7] M. Dur-e-Ahmad, W. Nicola, S.A. Campbell, and F.K. Skinner, *Network bursting using experimentally constrained single compartment CA3 hippocampal neuron models with adaptation*, J. Comput. Neurosci., 33 (2012), pp. 21–40.
[8] L. Hertag, D. Dustewitz, and N. Brunel, *Analytical approximations of the firing rate of an adaptive exponential integrate-and-fire neuron in the presence of synaptic noise*, Front. Comput. Neurosci., 8 (2014), 116.
[9] G.B. Ermentrout and D.H. Terman, *Mathematical Foundations of Neuroscience*, Springer, New York, 2010.
[10] G.B. Ermentrout, *Reduction of conductance-based models with slow synapses to neural nets*, Neural Comput., 6 (1994), pp. 679–695.
[11] G.B. Ermentrout and N. Kopell, *Parabolic bursting in an excitable system coupled with a slow oscillation*, SIAM J. Appl. Math., 46 (1986), pp. 233–253.
[12] J. Harris and G.B. Ermentrout, *Bifurcations in the Wilson–Cowan equations with nonsmooth firing rate*, SIAM J. Appl. Dyn. Syst., 14 (2015), pp. 43–72.
[13] D.J.W. Simpson, *Bifurcations in Piecewise-Smooth Continuous Systems*, World Scientific, Singapore, 2010.
[14] D.J.W. Simpson and J.D. Meiss, *Aspects of bifurcation theory for piecewise-smooth, continuous systems*, Phys. D, 241 (2012), pp. 1861–1868.
[15] F.D. Rossa and F. Dercole, *The transition from persistence to nonsmooth-fold scenarios in relay control system*, in Proceedings of the 18th IFAC World Congress, Milano, 2011, pp. 13287–13292.
[16] K.A. Ferguson, F. Njap, W. Nicola, F.K. Skinner, and S.A. Campbell, *Examining the limits of cellular adaptation bursting mechanisms in biologically-based excitatory networks of the hippocampus*, J. Comput. Neurosci. 39 (2015), pp. 289–309.
[17] K.A. Ferguson, C.Y.L. Huh, B. Amilhon, S. Williams, and F.K. Skinner, *Simple, biologically-constrained CA1 pyramidal cell models using an intact, whole hippocampus context*, F1000Research, 3 (2014), 104 (doi: 10.12688/f1000research.3894.1).
[18] D. Hansel and G. Mato, *Asynchronous states and the emergence of synchrony in large networks of excitatory and inhibitory neurons*, Neural Comput., 15 (2003), pp. 1–56.
[19] E.M. Izhikevich, *Simple model of spiking neurons*, IEEE Trans. Neural Netw., 14 (2003), pp. 1569–1572.
[20] Yu.A. Kuznetsov, S. Rinaldi, and A. Gragnani, *One-parameter bifurcations in planar Filippov systems*, Internat. J. Bifur. Chaos Appl. Sci. Engrg., 13 (2003), pp. 2157–2188.
[21] R. Naud, N. Marcille, C. Clopath, and W. Gerstner, *Firing patterns in the adaptive exponential integrate-and-fire model*, Biol. Cybernet., 99 (2008), pp. 335–347.
[22] W. Nicola, C. Ly, and S.A. Campbell, *One-dimensional population density approaches to recurrently coupled networks of neurons with noise*, SIAM J. Appl. Math. 75 (2015), pp. 2333–2360.
[23] W. Nicola and S.A. Campbell, *Bifurcations of large networks of two-dimensional integrate and fire neurons*, J. Comput. Neurosci., 35 (2013), pp. 87–108.
[24] D.Q. Nykamp and D. Tranchina, *A population density approach that facilitates large-scale modeling of neural networks: Analysis and an application to orientation tuning*, J. Comput. Neurosci., 8 (2000), pp. 19–50.
[25] A. Omurtag, B.W. Knight, and L. Sirovich, *On the simulation of large populations of neurons*, J. Comput. Neurosci., 8 (2000), pp. 51–63.
[26] J. Sotomayor, *Generic bifurcations of dynamical systems*, in Dynamical Systems, M.M. Peixoto, ed., Academic Press, New York, 1973, pp. 561–582.
[27] J. Touboul, *Bifurcation analysis of a general class of nonlinear integrate-and-fire neurons*, SIAM J. Appl. Math., 68 (2008), pp. 1045–1079.